

A novel *SMARCC1* BAFopathy implicates neural progenitor epigenetic dysregulation in human hydrocephalus

Amrita K. Singh,^{1,2,†} Garrett Allington,^{1,2,3,†} Stephen Viviano,⁴ Stephen McGee,⁵ Emre Kiziltug,^{1,2} Shaojie Ma,^{3,6} Shujuan Zhao,^{2,7} Kedous Y. Mekbib,^{1,2} John P. Shohfi,^{1,2} Phan Q. Duy,^{1,2,6} Tyrone DeSpenza Jr,^{1,2,6} Charuta G. Furey,¹ Benjamin C. Reeves,^{1,2} Hannah Smith,^{1,2} André M. M. Sousa,⁸ Adriana Cherskov,⁶ August Allocco,¹ Carol Nelson-Williams,³ Shozeb Haider,^{9,10} Syed R. A. Rizvi,⁹ Seth L. Alper,^{11,12,13} Nenad Sestan,^{3,4} Hermela Shimelis,¹⁴ Lauren K. Walsh,¹⁴ Richard P. Lifton,¹⁵ Andres Moreno-De-Luca,^{14,16} Sheng Chih Jin,⁷ Paul Kruszka,⁵ Engin Deniz⁴ and Kristopher T. Kahle^{2,11,17}

†These authors contributed equally to this work.

Abstract

Hydrocephalus, characterized by cerebral ventriculomegaly, is the most common disorder requiring brain surgery in children. Recent studies have implicated *SMARCC1*, a component of the BRG1-associated factor (BAF) chromatin remodeling complex, as a candidate congenital hydrocephalus (CH) gene. However, *SMARCC1* variants have not been systematically examined in a large patient cohort or conclusively linked with a human syndrome. Moreover, CH-associated *SMARCC1* variants have not been functionally validated or mechanistically studied *in vivo*. Here, we aimed to assess the prevalence of *SMARCC1* variants in an expanded patient cohort, describe associated clinical and radiographic phenotypes, and assess the impact of *Smarcc1* depletion in a novel *Xenopus tropicalis* model of CH. To do this, we performed a genetic association study using whole-exome sequencing from a cohort consisting of 2,697 total ventriculomegalic trios, including patients with neurosurgically-treated CH, that total 8,091 exomes collected over 7 years (2016-2023). A comparison control cohort consisted of 1,798 exomes from unaffected siblings of patients with autism spectrum disorder and their unaffected parents were sourced from the Simons simplex consortium. Enrichment and impact on protein structure were assessed in identified variants. Effects on the human fetal brain transcriptome were examined with RNA-sequencing and *Smarcc1* knockdowns were generated in *Xenopus* and studied using optical coherence tomography imaging, *in situ* hybridization, and

1 immunofluorescence. *SMARCC1* surpassed genome-wide significance thresholds, yielding six
2 rare protein-altering *de novo* variants (DNVs) localized to highly conserved residues in key
3 functional domains. Patients exhibited hydrocephalus with aqueductal stenosis; corpus callosum
4 abnormalities, developmental delay, and cardiac defects were also common. *Xenopus*
5 knockdowns recapitulated both aqueductal stenosis and cardiac defects and were rescued by
6 wild-type but not patient-specific variant SMARCC1. Hydrocephalic SMARCC1-variant human
7 fetal brain and *Smarcc1*-variant *Xenopus* brain exhibited a similarly altered expression of key
8 genes linked to midgestational neurogenesis, including the transcription factors *NEUROD2* and
9 *MAB21L2*. These results suggest DNVs in *SMARCC1* cause a novel human BAFopathy we term
10 “SMARCC1-associated Developmental Dysgenesis Syndrome (SaDDS)”, characterized by
11 variable presence of cerebral ventriculomegaly, aqueductal stenosis, DD, and a variety of
12 structural brain or cardiac defects. These data underscore the importance of SMARCC1 and the
13 BAF chromatin remodeling complex for human brain morphogenesis and provide evidence for a
14 “neural stem cell” paradigm of CH pathogenesis. These results highlight utility of trio-based
15 WES for identifying pathogenic variants in sporadic congenital structural brain disorders and
16 suggest WES may be a valuable adjunct in clinical management of CH patients.

17

18 **Author affiliations:**

19 1 Department of Neurosurgery, Yale University, New Haven, CT, 06510, USA

20 2 Department of Neurosurgery, Massachusetts General Hospital, Harvard Medical School,
21 Boston, MA, 02115, USA

22 3 Department of Genetics, Yale University, New Haven, CT, 06510, USA

23 4 Department of Pediatrics, Yale University, New Haven, CT, 06510, USA

24 5 GeneDx, Gaithersburg, MD, 20877, USA

25 6 Department of Neuroscience, Yale University, New Haven, CT, 06510, USA

26 7 Departments of Genetics and Pediatrics, Washington University School of Medicine, St Louis,
27 Missouri, 63110, USA

28 8 Waisman Center, University of Wisconsin-Madison, Madison, WI, 53705, USA

1 9 Department of Pharmaceutical and Biological Chemistry, University College London School
2 of Pharmacy, London, WC1N 1AX, UK

3 10 UCL Centre for Advanced Research Computing, University College London, WC1H 9RN,
4 UK

5 11 Broad Institute of MIT and Harvard, Cambridge, MA, 02142, USA

6 12 Division of Nephrology and Vascular Biology Research Center, Beth Israel Deaconess
7 Medical Center, Boston, MA, 02215, USA

8 13 Department of Medicine, Harvard Medical School, Boston, MA, 02115, USA

9 14 Autism & Developmental Medicine Institute, Geisinger, Danville, PA, 17822, USA

10 15 Laboratory of Human Genetics and Genomics, The Rockefeller University, New York, NY,
11 10065, USA

12 16 Department of Radiology, Diagnostic Medicine Institute, Geisinger, Danville, PA, 17822,
13 USA

14 17 Division of Genetics and Genomics, Boston Children's Hospital, Boston, MA, 02115, USA

15

16 Correspondence to: Kristopher T. Kahle, MD, PhD

17 Massachusetts General Hospital and Harvard Medical School

18 Department of Neurosurgery

19 55 Fruit St., Wang Ambulatory Care Center, Suite 333

20 Boston, MA 02114, USA

21 E-mail: kahle.kristopher@mgh.harvard.edu

22

23 **Running title:** *SMARCC1* in human hydrocephalus

24 **Keywords:** congenital; neurodevelopment; chromatin; neurosurgery; genetics; genomics

25

1 Introduction

2 Epigenetic mechanisms, including methylation, histone modifications, and ATP-dependent
3 chromatin remodeling, regulate gene expression by altering chromatin structure.¹⁻⁴ The SWI/SNF
4 (SWItch/Sucrose Non-Fermentable) complex (also known as the BRG1-associated factor [BAF]
5 complex) is one of four ATP-dependent chromatin remodeling complexes known in mammals.⁵⁻⁷
6 The BAF complex mediates nucleosome modification critical to modulating gene expression in
7 multiple essential processes, including cell differentiation and proliferation, and DNA repair.¹⁻⁵
8 The combinatorial assembly of numerous gene family paralogs yields many potential types of
9 complex hetero-oligomeric complexes that provide tissue and temporal specificity⁶⁻⁸ for the
10 control of gene transcription that is essential for the development of the brain,^{9,10} heart,¹¹⁻¹³ and
11 other organs, as well as the maintenance of embryonic stem cell pluripotency (Table 1).¹⁴

12
13 BAFopathies constitute a heterogeneous group of disorders caused by variants in various
14 subunits composing the BAF complex.¹⁵ The phenotypic spectrum of BAFopathies includes
15 intellectual disability (ID) and developmental delay (DD), autism, schizophrenia, amyotrophic
16 lateral sclerosis,²⁰⁻²² and other human neurodevelopmental disorders and anatomical congenital
17 defects.^{16,17} The most recognizable syndrome associated with BAF abnormalities is Coffin-Siris
18 syndrome (CSS [MIM: 135900]). This is a genetically heterogeneous ID/DD syndrome
19 characterized by speech delay, coarse facial appearance, feeding difficulties, hypoplastic-to-
20 absent fifth fingernails, and fifth distal phalanges.¹⁸ This syndrome is associated with variants in
21 multiple BAF complex subunits, including the ATPase subunit *SMARCA4* (MIM: 603254), the
22 common core subunit *SMARCB1* (MIM: 601607), and BAF accessory subunits such as
23 *SMARCE1/BAF57* (MIM: 603111), *ARID1A* (MIM: 603024), *ARID1B* (MIM: 614556), *ARID2*
24 (MIM: 609539), and *DPF2* (MIM: 601671).^{18,19} Other BAFopathies, such as Nicolaides-
25 Baraitser syndrome (MIM: 601358), have significant phenotypic overlap with CSS and are
26 caused by pathogenic variants in *SMARCA2* (MIM: 600014).²⁰⁻²²

27
28 *SMARCC1* (SWI/SNF-Related, Matrix-Associated, Actin-Dependent Regulator Of Chromatin
29 Subfamily C Member 1) encodes an essential core subunit of the BAF complex highly

1 homologous to *SMARCC2*.^{8,23} *Smarcc1* is highly expressed in the mouse embryonic
2 neuroepithelium and ventricular zone.^{9,10,14} Similar to other components of the neuroprogenitor-
3 specific BAF complexes, *Smarcc1* regulates the proliferation, differentiation, and survival of
4 mouse neural progenitors via transcriptional regulation of genes critical for telencephalon
5 development.²⁴⁻²⁷ *Smarcc2*; *Smarcc1* double knockout mice exhibit proteasome-mediated
6 degradation of the entire BAF complex, resulting in impairment of the global epigenetic and
7 gene expression program of cortical development.^{15,28} *Smarcc1* knockout causes embryonic
8 lethality in mice.^{29,30} ~80% of mice homozygous for the *Smarcc1*^{msp/msp} missense allele exhibit
9 exencephaly due to decreased proliferation and increased apoptosis of neural progenitors in the
10 neural tube.^{29,31}

11
12 Recently, whole-exome sequencing (WES) studies in patients with congenital hydrocephalus
13 (CH) identified *SMARCC1* as a candidate gene, implicating impaired epigenetic regulation of
14 neural progenitor cell (NPC) proliferation and differentiation in the development of
15 ventriculomegaly.^{32,33} However, despite its significant biological role, *SMARCC1* variants have
16 not been conclusively associated with a human syndrome, and CH-associated *SMARCC1*
17 variants have been neither functionally assessed nor mechanistically studied *in vivo*. The
18 objectives of this study were to: (i) assess the prevalence of rare, damaging DNVs in *SMARCC1*
19 in a large CH cohort; (ii) describe the phenotypes of *SMARCC1*-variant patients; and (iii)
20 functionally-validate and assess the cellular and molecular mechanisms of CH-associated
21 *SMARCC1* variants in a novel animal model of hydrocephalus.

22
23 Our findings suggest rare, damaging germline DNVs in *SMARCC1* cause a novel human
24 BAFopathy we term “*SMARCC1*-associated Developmental Dysgenesis Syndrome (SaDDS)”
25 characterized by DD, cerebral ventriculomegaly, and other structural brain or cardiac defects.
26 Our data highlight the importance of the ATP-dependent BAF chromatin remodeling complex
27 for human brain morphogenesis and CSF dynamics and further support a “neural stem cell
28 paradigm” of human CH.³⁴⁻³⁶ These data highlight the power of trio-based WES for identifying
29 pathogenic variants in sporadic structural brain disorders and suggest its utility as a prognostic
30 adjunct when evaluating the surgical candidacy and prognosis of CH patients.

1 **Materials and methods**

2 **Patient cohort**

3 All study procedures and protocols were guided by and in compliance with Human Investigation
4 Committee and Human Research Protection Program at Yale School of Medicine and the
5 Massachusetts General Hospital. All participants provided written, informed consent to
6 participate in accordance with the Declaration of Helsinki. For patients from the clinical
7 laboratory GeneDx, denoted CHYDX, written informed consent for genetic testing was obtained
8 from the guardians of all pediatric individuals undergoing testing. The Western institutional
9 review board waived authorization for the use of de-identified aggregate data for the purposes of
10 this study. Criteria for inclusion into the study was congenital or primary cerebral
11 ventriculomegaly, including congenital hydrocephalus. Patients and participating family
12 members provided buccal swab samples (Isohelix SK-2S DNA buccal swab kits), medical
13 records, neuroimaging studies, operative reports, and phenotype data when available. Human
14 phenotype ontology terms were used to aggregate relevant pediatric patients in the GeneDx
15 database. The comparison control cohort consisted of 1,798 unaffected siblings of people
16 diagnosed with autism spectrum disorder (ASD) and unaffected parents sourced from the Simons
17 simplex consortium (SSC)³⁷. Only the unaffected siblings and parents, as designated by SSC,
18 were included in the analysis, and served as controls for this study. Permission to access the
19 genomic data in the SSC on the National Institute of Mental Health Data Repository was
20 obtained. Written and informed consent for all participants was provided by the Simons
21 Foundation Autism Research Initiative.

22

23 **Kinship analysis**

24 Pedigree information and relationships between proband and parents was confirmed using
25 pairwise PLINK identity-by-descent (IBD) calculation.³⁸ The IBD sharing between the probands
26 and parents in all trios was between 45% and 55%. Pairwise individual relatedness was
27 calculated using KING³⁹. The ethnicity of each patient from the Yale cohort was determined by
28 single-nucleotide polymorphisms in cases, controls, and HapMap samples using EIGENSTRAT,

1 as previously described.⁴⁰ For the GeneDx cohort, kinship analysis was performed using an
2 internally developed KNN/PCA pipeline.

3

4 **WES and variant calling**

5 Patient genomic DNA samples derived from saliva or blood were applied for exon capture using
6 Roche SeqCap EZ MedExome Target Enrichment kit or IDT xGen target capture followed by
7 101 or 148 base-paired-end sequencing on Illumina platforms as described previously^{32,33}. BWA-
8 MEM was applied to align sequence reads to the human reference genome GRCh37/hg19.
9 Single-nucleotide variants and small indels were called using a combination of GATK
10 HaplotypeCaller and Freebayes^{41,42} and annotated using ANNOVAR⁴³. The cDNA change and
11 protein change were accurately annotated using transcript variant NM_003074.4 and protein
12 isoform NP_003065.3, respectively. Allele frequencies were annotated in the Exome
13 Aggregation Consortium, GnomAD (v.2.1.1) and Bravo databases.⁴⁴ Variant filtration and
14 analysis were conducted following GATK best practices and consensus workflows.⁴⁵ MetaSVM
15 and MPC algorithms were used to predict the deleteriousness of missense variants (D-mis,
16 defined as MetaSVM-deleterious or MPC-score ≥ 2).⁴⁶ Inferred loss-of-function (LoF) variants
17 consisted of stop-gain, stop-loss, frameshift insertions/deletions, canonical splice site and start-
18 loss. LoF and D-Mis variants were considered 'damaging'. Analyses were conducted separately
19 for each class of variant – DNVs and rare, heterozygous variants – following previously
20 established analytical methodologies^{33,45}. Firstly, DNVs from the Harvard-Yale cohort were
21 called from all CH parent-offspring trios using the established TrioDeNovo pipeline^{47,48}. GeneDx
22 DNVs were called as previously defined.⁴⁹ Candidate DNVs for all samples were further filtered
23 based on whether the variants were called in the exonic or splice-site regions, the variant read
24 depth (DP) was at least ten in the proband as well as both parents, and the global minor allele
25 frequency was less than or equal to 4×10^{-4} in the Exome Aggregation Consortium database.
26 Samples from the Yale cohort were subsequently filtered based on the following criteria: (i) the
27 proband's alternative read depth was greater than or equal to five; (ii) proband alternative allele
28 ratio greater than or equal to 28% if having less than ten alternative reads, or less than or equal to
29 20% if having greater than or equal to ten alternative reads; (iii) the alternative allele ratio in
30 both parents less than or equal to 3.5%. Samples from the GeneDx cohort were additionally

1 filtered based on the following criteria: (i) Genotype quality (GQ) > 40 for all family members;
2 (ii) Variant quality score log odds (VQSLOD) > -10; (iii) Phred-scaled p-value (Fishers exact
3 test; FS) <30; (iv) Proband alternate allele count >4; (v) Proband alternate allele ratio > 0.1; (vi)
4 Proband alternate allele ratio >0.15 if REF and ALT calls are of equal length; (vii) Proband
5 alternate allele ratio >0.25 if REF and ALT calls are of unequal length; (viii) Proband alternate
6 allele ratio < 0.9 in proband if DNV is autosomal; (ix) DNV must be < 100 bps in size for both
7 the REF and ALT calls; (x) If the VQSLOD <7 and the alternate allele ratio in the proband <0.3,
8 the variant was omitted. (xi) DNVs were omitted if they existed in more than 2 unrelated
9 probands. After filtering as above, *in silico* visualization was performed, applying in-house
10 software to manually inspect each variant for false-positive calls. Variants found to be false-
11 positive upon manual inspection were removed. *SMARCC1* variant annotations were then
12 confirmed through manual cross-reference in the UCSC Genome Browser.^{43,50} Reported variants
13 passing these filters and manual inspection in *SMARCC1* were further confirmed by Sanger
14 sequencing.

15

16 **Developmental human brain scRNA-seq dataset analysis**

17 As described previously²⁴, the preprocessing and clustering analysis for scRNA developmental
18 human brain dataset was completed using Seurat.⁵¹ Briefly, cells with fewer than 1000 genes/cell
19 were removed, as were cells with greater than 10% of their individual transcriptome represented
20 in either mitochondrial or ribosomal transcripts. Only genes expressed in at least 30 cells were
21 carried forward in the analysis. The raw counts were normalized and log2 transformed by first
22 calculating ‘size factors’ that represented the extent to which counts should be scaled in each
23 library. Highly variable genes were detected using the proposed workflow of and were
24 subsequently used for unsupervised dimensionality reduction techniques and principal
25 component analysis. UMAP coordinates were calculated using standard Seurat workflow, and
26 clusters were assigned to cells based on previous analysis via a hybrid method using Louvain
27 clustering and WGCNA.²⁴ Non-parameteric Wilcoxon rank sum test was used to identify
28 differentially expressed markers across time points, areas and laminar zones by running
29 FindAllMarkers. Heatmap expression values were calculated using AverageExpression function
30 and visualization of the heatmaps were created using pheatmap package.

1 **Cell type enrichment**

2 Cell type enrichment for the expression of SMARCC1 was tested in scRNA-seq datasets of
3 prenatal human brain using in-house custom-made script in R studio^{52,53}. Enrichment for each
4 cell type was tested using hypergeometric test, where a gene list was significantly enriched in a
5 cell type if the adjusted p value was less than 0.05. Average expression was shown using the
6 DotPlot function from the Seurat package. For control comparison, we used frontal neocortex
7 layer-specific data from the BrainSpan database matched by developmental age.⁵² Batch
8 correction was applied by quantile normalization in the limma package.⁵⁴ Median fold changes
9 of gene expression were used to rank the genes. Only protein-coding genes were used for
10 analysis.

11

12 ***SMARCC1* expression in PsychENCODE bulk RNA sequencing**

13 To examine the expression pattern of SMARCC1 during human brain development, we extracted
14 Reads Per Kilobase per Million (RPKM) expression from the PsychENCODE bulk tissue RNA
15 sequencing dataset.⁵³ Gene expression was scaled, centered and average values calculated across
16 developmental periods. The expression distributions were visualized in a violin plot.

17

18 **Gene Ontology (GO) enrichment analysis**

19 To test for functional enrichment for all modules and the respective genes, we performed gene
20 ontology enrichment analysis (GOEA) for using the GO set of biological processes. Gene set
21 ‘GO.v5.2.symbols_mouse.gmt’ was obtained from the Molecular Signatures Database. The
22 compareCluster and enrichGo functions from the R package ClusterProfiler (version 3.12.0)
23 were used to determine significant enrichment ($q < 0.05$) of biological processes. All present
24 genes were used as background (universe). To focus only on neurological gene sets, GO term
25 gene sets were selected for terms including the term ‘neuro’, ‘neural’ and ‘nerv’. Network
26 visualization was performed using the cnetplot function from the R package ClusterProfiler.

27

1 **Acquisition, pre-processing, and differential gene expression analysis of post-** 2 **mortem tissue**

3 A stillborn male fetus was born at Medstar Washington Hospital Center via induced vaginal
4 delivery at a clinical gestation age of 20 weeks for pregnancy termination due to sonographic and
5 MRI findings of supratentorial ventriculomegaly/and hydrocephalus suggestive of aqueductal
6 stenosis. The mother had a previous history of pregnancy termination at 22 weeks due to a
7 similar fetal anomaly. The patient underwent autopsy assessment at Children's National Medical
8 Center at the request of the parents, which identified body weight, crown- rump length, crown-
9 heel length, foot length, and organ weights consistent with 20-23 weeks gestation.
10 Representative sections of the cortex, brainstem, and cerebellum were retained for analysis at the
11 request of and with the written consent of the patient's parents. Written informed consent for de-
12 identified genetic testing of samples from the patient and direct family members was obtained.
13 All written consent was obtained in accordance with the Declaration of Helsinki and in
14 compliance with the Human Investigation Committee at Yale University.

15
16 Both the patient and the patient's mother were found to have an amino acid substitution in
17 *SMARCC1* c.1723C>T, yielding p.Gln575*. Tissue processing was performed using the Genra
18 Puregene Tissue Kit. The *SMARCC1* bulk-tissue RNA-seq data were then aligned to the hg38
19 genome assembly and GENCODE v21 gene annotation using STAR, followed by read counting
20 via HTSeq. The count data were then used to compute RPKM in accordance with methods used
21 in the BrainSpan dataset⁵³, enabling downstream gene expression comparisons between these
22 two datasets.

23
24 We used gestational age-matched neocortical samples from the BrainSpan dataset to identify up-
25 and down-regulated genes in the *SMARCC1*-variant cortex. For the downstream analysis, we
26 examined only protein coding genes, and further removed mitochondria and histone genes as
27 these could bias the analysis. Since there was only one cortical sample available, traditional
28 differential gene expression analysis would not be feasible. As an alternative, we performed
29 pairwise comparisons between the *SMARCC1* neocortical data and the data of each neocortical

1 area in BrainSpan, and calculated the expression fold changes, with a pseudo-value of 1 added to
2 both numerators and denominators. The median expression fold changes among these pairwise
3 comparisons were compared. To identify the most robust changes, we set the threshold of fold
4 changes at \log_5 for the upregulated genes and $-\log_5$ for the downregulated genes. GOEA was
5 performed on the top 200 up- and down-regulated genes using the topGO package in R⁵⁵, and
6 the significant terms were selected with a false discovery rate (FDR) cutoff of 0.01.

8 *Xenopus* husbandry

9 *Xenopus tropicalis* were raised and cared for in our aquatics facility according to protocols
10 approved by the Yale University Institutional Animal Care and Use Committee. Embryos were
11 staged according to Nieuwkoop and Faber⁵⁶.

13 sgRNA and RNA production

14 CRISPR: Two non-overlapping CRISPR sgRNAs were designed on crisprscan.org for the
15 *Xenopus tropicalis smarcc1* gene (Xenbase genome v9.1) and produced using an EnGen sgRNA
16 Synthesis Kit (NEB # E3322). Target sites are located in exon #10 (CRISPR #1: 5'-
17 AGGCTGTGCGCAGTCCCGAGAGG-3'), and exon 1 (CRISPR #2: 5'-
18 CGGCCGGGAAGAGCCCCGAGGG-3'). CRISPR indels were verified by performing Sanger
19 sequencing on PCR products using genomic DNA from stage 46 embryos. Genomic DNA was
20 extracted from individual anesthetized embryos at phenotypic stage 46 by 10 minute incubation
21 in 50ul of 50mM NaOH at 95°C followed by neutralization with 20ul of 1M Tris pH 7.4. PCR
22 was performed with either Phusion High-Fidelity DNA Polymerase (NEB #M0530) (CRISPR
23 #1), or Platinum SuperFi II Green PCR Master Mix (Thermo Fisher Scientific #12369050)
24 (CRISPR #2) using primers around the CRISPR cut site (CRISPR #1: 5'-
25 ACATTGGTCCCTGTGCTTTT-3' and 5'-TTCAAGTCCTCGTCTGTTTGG-3', CRISPR #2:
26 5'-AACGGCAGCAATAACGGAGA-3' and 5'-AGATACATGTCCCCTCCGCA-3'). PCR
27 sequences were analyzed for indels using the online Inference of CRISPR Edits (ICE) tool
28 (Synthego).

1 Human mRNA: Human SMARCC1 mRNA was produced by cloning a full length insert
2 (sequence ID NM_003074.4) into a pCS DEST expression plasmid backbone using Gateway
3 recombination techniques. mRNA was synthesized using a mMACHINE SP6
4 Transcription Kit (Thermo Fisher Scientific #AM1340). The patient variant 1723T>C (p. Q575*)
5 was produced using inverse PCR. Overlapping primers [forward and reverse] were designed with
6 the base change located in the middle, with 14 bases on either side of the variant. Long range
7 PCR was performed with wild-type plasmid template using Platinum Taq DNA Polymerase High
8 Fidelity (Thermo Fisher Scientific # 11304011). DpnI digestion removed methylated template
9 DNA from nonmethylated PCR product, which was then used to transform Ca²⁺-competent E.
10 Coli. Individual clones were grown up, and plasmid DNA was extracted and sequenced to verify
11 the presence in the insert of only the desired variant. The insert was cloned into a pCS DEST
12 expression vector and mRNA was synthesized as above.

13

14 **Microinjection, gene expression, knockdown and overexpression**

15 *Xenopus tropicalis* embryos were microinjected using standard protocols.⁵⁷⁻⁵⁹ Fertilized eggs
16 were injected at either 1 cell stage with a 2 nl volume, or into 1 of 2 cells at 2 cell stage with a 1
17 nl volume. Injection mixes for expression knockdown using morpholino oligo (MO) consisted of
18 the fluorescent tracer Dextran Alexa Fluor 488 (Thermo Fisher Scientific #D22910) along with
19 MO targeting the start site of *Xenopus tropicalis smarcc1* (gene model XM_002942718.5) (5'-
20 CCTTTGTTTCATGGCTGCTACTCCC-3', Gene Tools) at a concentration leading to a dose of
21 0.5-1.0ng per embryo. A standard control MO (5'-CCTCTTACCTCAGTTACAATTTATA-3',
22 Gene Tools) was also used at the same dose. We also used CRISPR/Cas9-mediated gene editing
23 for expression knockdown as previously described⁶⁰. CRISPR injection mixes consisted of
24 fluorescent tracer, and the following components at a concentration leading to the listed dose per
25 embryo: 1.6 ng Cas9 (CP03, PNA Bio), 400pg sgRNA. 500 pg mRNA encoding human wild
26 type or patient variant protein was injected into each embryo to rescue MO knockdown.
27 Injections were verified using a Zeiss SteREO Lumar.V12 microscope to visualize fluorescence
28 at stages 18-46 in the entire embryo (1 cell injection), or on only the right or left side (2 cell
29 injection).

30

1 **Optical coherence tomography imaging**

2 A Thorlabs Ganymede II HR OCT imaging system using ThorImage OCT version 5.0.1.0
3 software was used to obtain 2D cross-sectional images and movies. Imaging was obtained as
4 previously described.⁵⁸

6 **Western blotting**

7 Whole cell lysate was extracted from pooled embryos in RIPA lysis buffer (Millipore #20-188)
8 supplemented with Halt protease and phosphatase inhibitor cocktail (Thermo Fisher Scientific
9 #78440). Samples were run on Bolt 4-12% Bis-Tris Plus gels (Thermo Fisher Scientific) then
10 transferred to PVDF membranes. Immunoblotting was performed using standard methods.
11 Polyclonal rabbit anti-SMARCC1 antibody (Thermo Fisher Scientific #PA5-96513) was used at
12 1:1000, and mouse anti- β -Actin (C4) HRP (Santa Cruz Biotechnology #sc47778) was used at
13 1:100,000 as a loading control.

15 **Whole mount *in situ* hybridization**

16 Whole mount *in situ* hybridization (WISH) was performed as previously described⁶¹. Briefly,
17 *Xenopus tropicalis* embryos were fixed in 4% paraformaldehyde in 2mM EGTA, then
18 dehydrated through methanol washes and stored at -20°C. Embryos were rehydrated through
19 washes in PBS + 0.1% tween-20, then incubated in 4% hydrogen peroxide in PBS + 0.1%
20 Tween-20 to remove pigment. After post-fixing in 4% paraformaldehyde in 2mM EGTA,
21 embryos were hybridized overnight at 60°C with RNA probes. The Digoxigenin-11-UTP (Sigma
22 #11209256910) labeled RNA probes were produced with full length insert containing expression
23 plasmids using either HiScribe T7 (antisense), or HiScribe SP6 (sense) RNA Synthesis Kits
24 (NEB) according to the manufacturers' instructions (Table 2).

25 After overnight hybridization, embryos were washed, blocked, then incubated overnight in Anti-
26 Digoxigenin-AP, Fab fragments (Sigma #11093274910). After washes, embryos were incubated
27 in BM Purple (Sigma # 11442074001) until signal was fully visible, then fixed in 4%
28 paraformaldehyde + 0.1% glutaraldehyde in 2mM EGTA.

1 **Immunohistochemistry**

2 Uninjected control, 1 of 2 cell control MO-, or 1 of 2 cell smarcc1 MO-injected stage 47
3 embryos were anesthetized, then fixed in 4% paraformaldehyde in PBS for 1 hour at room
4 temperature. After washes in PBS, tails, guts, and ventral structures of the head including lower
5 jaws and facial cartilage were removed. Pigment was bleached from samples by incubation in
6 5% formamide + 1.2% H₂O₂ in PBS while exposed to light. Samples were then washed with PBS
7 + 0.1% Triton X-100 (PTr), blocked in 10% CAS-Block (Thermo Fisher Scientific #008120) in
8 PTr, then incubated in mouse monoclonal anti-PCNA (PC10) (Thermo Fisher Scientific #13-
9 3900) diluted 1:200 in 100% CAS-Block overnight at 4°C. After extensive washes in PTr,
10 samples were blocked in 10% CAS-Block, then incubated overnight at 4°C in Texas Red-
11 conjugated goat anti-mouse IgG (Thermo Fisher Scientific #T-6390) plus Hoechst 33342
12 (Thermo Fisher Scientific #H3570), respectively diluted 1:200 and 1:5000 in 100% CAS-Block.
13 Samples washed first in PTr, then in PBS, were mounted between two coverslips in ProLong
14 Gold Antifade Mountant (Thermo Fisher Scientific #P36934). Images were obtained using a
15 Zeiss LSM 880 airyscan confocal microscope.

17 **RNA sequencing analysis**

18 Sequenced reads were aligned and quantified using STAR: ultrafast universal RNA-seq aligner
19 (version 2.7.3a) and the murine reference genome, GRCm38p5, from the Genome Reference
20 Consortium. Raw counts were imported using the DESeqDataSetFromHTSeqCount function
21 from DESeq2 (version 1.26.0) and rlog-transformed according to the DESeq2 pipeline. DESeq2
22 was used for calculation of normalized counts for each transcript using default parameters. All
23 normalized transcripts with maximum overall row mean < 20 were excluded, resulting in 13,284
24 present protein-coding transcripts. Undesired or hidden causes of variation, such as batch and
25 preparation date, were removed using the sva package. The normalized rlog-transformed
26 expression data were adjusted with four surrogate variables identified by sva using the function
27 removeBatchEffect from the limma package. To determine gene clusters, CoCena (Construction
28 of Co-expression network analysis) was calculated based on Pearson correlation on all present
29 genes. Pearson correlation was performed using the R package Hmisc (version 4.1-1). To
30 increase data quality, only significant ($P < 0.05$) correlation values were kept. A Pearson

1 correlation coefficient cutoff of 0.803 (present genes; 10,260 nodes and 69,986 edges) was
2 chosen, resulting in networks following the power-law distribution of $r^2 = 0.934$ (scale-free
3 topology). Unbiased clustering was performed using the ‘leiden modularity’ algorithm in igraph
4 (version 1.2.1). Clustering was repeated 100 times. Genes assigned to more than ten different
5 clusters received no cluster assignment. The mean group fold change expression for each cluster
6 and condition is visualized in the Cluster/Condition heat map. Clusters smaller than 40 genes are
7 not shown.

8
9 Single-cell gene expression from age-matched *Smarcb1*-mutant (n=44,755) and wild-type (n=27,
10 230) mouse brains was obtained from a publicly available dataset of cells (Gene Expression
11 Omnibus: GSE212672). Seurat version 4.0.3 was used to cluster cells based upon previously
12 described cell types. The resulting Seurat object was then imported into Monocle 3 version
13 0.2.3⁶². A Monocle 3 cell dataset was constructed and a Moran’s I test was applied to identify
14 differential gene expression in the cell dataset based on low dimensional embedding and the
15 principal graph with neighbor graph=knn, reduction method = UMAP, k=25,
16 alternative = greater, method = Moran_I and expression_family = quasipoisson. To infer cell-cell
17 interactions based on the expression of known ligand-receptor pairs in different cell types,
18 CellChat⁶³ was applied. The official workflow and databases were implemented. Briefly, the
19 normalized counts were loaded into CellChat, after which the preprocessing functions
20 identifyOverExpressedGenes, identifyOverExpressedInteractions and project Data with standard
21 parameters set were applied. The main analyses were conducted using the functions
22 computeCommunProb, computeCommunProbPathway and aggregateNet with fixed
23 randomization seeds.

24

25 **Statistics and reproducibility**

26 No power analysis was performed to predetermine sample size, as our sample sizes are similar to
27 those reported in previous publications^{32,33,64}. Randomization was not relevant to this study as
28 controls and *X. tropicalis* knockdowns did not receive different treatments and human studies
29 were descriptive studies. All experiments were performed and analyzed in a blinded manner. No
30 data were excluded from the analyses. Wilcoxon Rank-Sum test was used in differential gene

1 expression analysis, as described in Methods. Mann-Whitney test was used to analyze
2 experimental data in Figure 3c. Elsewhere, data distribution was assumed to be normal, but this
3 was not formally tested.

5 Results

6 The total sequenced cohort consisted of a of 8,091 exomes (2,697 trios) with cerebral
7 ventriculomegaly. This included 2,416 new trios from a clinical referral cohort (GeneDx) and
8 281 trios from an academic neurosurgical cohort (Harvard-Yale) (see Methods). Among the
9 latter, 49 new trios were added to a cohort previously described.^{32,33} The control cohort consisted
10 of 1,798 exomes from unaffected siblings of people diagnosed with autism spectrum disorder
11 and their unaffected parents sourced from the Simons simplex consortium.^{32,65} Genomic DNAs
12 were subjected to WES, and variant calling was performed with GATK HaplotypeCaller and
13 Freebayes followed by ANNOVAR annotation and confirmation by the Integrative Genomics
14 Viewer.^{33,43,50} Reported variants were confirmed by Sanger sequencing.

15
16 We compared observed and expected numbers of non-synonymous DNVs in all genes in cases
17 and controls (see Methods). In the Harvard-Yale cohort, three missense or loss-of-function
18 variants in *SMARCC1* were identified, yielding a protein-altering DNV burden of 3.92×10^{-8}
19 that surpassed the threshold for exome-wide significance (multiple-testing correction threshold
20 of 8.57×10^{-7} after correction for testing 19,347 RefSeq genes in triplicate using a one-tailed
21 Poisson test. These variants included the previously described variants p.His526Pro,
22 p.Lys891Argfs*6, and c.1571+G>A variants (Table 1).^{32,33} In the GeneDx cohort, three new
23 protein-altering DNVs in *SMARCC1* were identified, including the c.2204A>G (p. Asp675Gly),
24 c.170delT (p. Val57Alafs*97), and recurrent c.1571+1G>A variants, yielding a DNV burden of
25 7.39×10^{-4} . Based on the presence of six total DNVs in the Harvard-Yale and GeneDx cohorts
26 (2,697 total patient-parent trios), *SMARCC1* carried a protein-altering DNV burden of 5.83×10^{-9} ,
27 surpassing the threshold for exome-wide significance (Fig. 1a). Among *SMARCC1* non-
28 synonymous missense DNVs, p.His526Pro is predicted to abolish interaction with the backbone
29 carbonyl oxygen of p.Leu505 at the end of an adjacent helix in the SWIRM domain mediating

1 BAF complex subunit interactions.⁶⁶ p.Asp675Gly alters a conserved residue in the Myb domain
2 resulting in an unfavorable loss of an ion pair interaction with p.Arg602 (Fig. 1c). All these
3 DNVs are absent in gnomAD and Bravo databases.

4
5 We examined the clinical phenotypes of probands harboring *SMARCC1* DNVs and other
6 published rare, damaging transmitted or unknown inheritance CH-associated *SMARCC1*
7 variants³³ (Table 3). The latter included two transmitted LoF variants (p.Gln575* and
8 p.Val535Serfs*29), one unknown inheritance rare LoF variant (p.Thr415Lysfs*29), and one
9 transmitted rare damaging missense (D-Mis) variant (p.Arg652Cys). Strikingly, 10/10 had
10 perinatally diagnosed cerebral ventriculomegaly, and at least 7 required neurosurgical CSF
11 diversion by endoscopic third ventriculostomy or ventriculoperitoneal shunting. 9/10 had
12 aqueductal stenosis. 9/10 had partial or complete corpus callosum abnormalities, including septal
13 agenesis. 9/10 exhibited moderate to profound DD. 9/10 had cardiac defects including atrial
14 septal defect, ventricular septal defect, double outlet right ventricle, and cardiac hypoplasia.
15 Other neurodevelopmental phenotypes, such as seizures, structural brain defects like cerebellar
16 tonsillar ectopia, and craniofacial defects including cleft palate, microtia, and auditory canal
17 atresia were variably present (Table 3, Fig. 1d). These data suggest that *SMARCC1* variants, in
18 addition to conferring CH risk, leads to a novel human syndrome with phenotypes that resemble
19 other BAFopathies.^{20,21,67,68}

20
21 We also examined the clinical phenotypes of 13 individuals reported in the literature with rare,
22 damaging *SMARCC1* DNVs or transmitted variants (Supplementary Table 3), including four
23 damaging *de novo* variants (p.Gln742Arg, p.Trp279*, p.Trp279*, c.2782-1G)⁶⁹⁻⁷¹, four inherited
24 damaging variants (p.Arg912*, p.Gln972Sfs*19, p.Gln956*, p.Lys615Ilefs*49^{72,73}, two
25 damaging variants (p.Gln1005*, p.Asp821Glufs*4) of unknown inheritance and two exon
26 deletions (deletion of exon 4 and deletion of exon 4-6)⁶⁸ unknown inheritance. Interestingly, the
27 patient with the *de novo* c.2782-1G variant had CH and aqueductal stenosis along with
28 appendicular skeletal defects. Among the patients, 6/12 patients had developmental delay, 4/12
29 had autism spectrum disorder, and 3/12 patients had craniofacial defects and appendicular
30 skeletal defects (as well as scoliosis and vertebral defects). Other developmental abnormalities

1 included polymicrogyria, attention deficit hyperactivity disorder, and seizures. These findings
2 are consistent with the phenotypes of our cohort and further expand *SMARCC1* phenotypic
3 spectrum.

4
5 *Smarcc1* is expressed in mouse ventricular zone neuroepithelial and neural progenitor cells
6 during midgestation,^{10,32,74,75} a key epoch during which neurogenesis contributes to the
7 development of the diencephalon and telencephalon.^{9,24,29,75-78} We studied the expression of
8 *SMARCC1* in the human brain during development using single-cell RNA-sequencing database
9 of 4,261 cells from developmental human whole brain tissue during PCW 6-40.²⁴ We found that
10 *SMARCC1* and other BAF complex genes are expressed highly in intermediate progenitor cells
11 (IPCs) between PCW 13-20. (Fig. 2a-2d). In addition, *SMARCC1* is highly expressed in the
12 lateral ganglionic eminence, a NPC niche within the ventral telencephalon that harbors NPCs
13 destined for cortical and striatal interneurons and oligodendrocyte precursor cells (OPCs) (Fig.
14 2e).⁷⁹ When investigating ventricular lamina expression, we found that BAF complex members
15 are also expressed throughout the ventricular laminae. Further, *SMARCC1* is most highly
16 expressed in the ventricular zone (Figure 2f). These data show that *SMARCC1* is highly
17 expressed in human fetal periventricular NPCs.

18
19 To functionally validate *SMARCC1* as a novel disease gene, we generated *Smarcc1* mutant
20 *Xenopus tropicalis* tadpoles since mice with *Smarcc1* deletion are embryonic lethal.²⁹⁻³¹
21 Additionally, brain morphogenesis and CSF circulation can be studied in live *Xenopus* tadpoles
22 using optical coherence tomography (OCT) (Supplementary Fig. 1).^{80,81} We knocked down
23 *Xenopus Smarcc1* using CRISPR/CAS9 targeting exon1 and exon10, as well as by using a
24 morpholino oligo targeting the *Smarcc1* transcription start site (Fig. 3a, 3b, Supplementary Fig.
25 2). All three resulting *Smarcc1* mutant and morphant tadpoles exhibited highly penetrant
26 aqueductal stenosis that was transmitted to G1 mutant progeny (Fig. 3a, 3b). Despite this, OCT
27 imaging demonstrated intact ependymal cilia-driven CSF circulation (Supplementary Fig. 3).
28 Overexpression of human wild-type *SMARCC1* but not human CH-variant *SMARCC1* p.Gln575*
29 in *Smarcc1*-depleted *X. tropicalis* variants (see Methods) rescued aqueductal stenosis (Fig. 3c,
30 Supplementary Fig. 4). *Smarcc1*-depleted variants also exhibited decreased cardiac function

1 resembling hypoplastic cardiomyopathy (e.g., see proband CHYD111-1), as quantified by end-
2 diastolic diameter and end-systolic diameter (Fig. 3d-3g). These results show CH-associated
3 *SMARCC1* variants or *Smarcc1* depletion in *Xenopus* phenocopies the core brain and cardiac
4 pathology of humans with *SMARCC1* variants.

5
6 To begin to elucidate the cellular pathogenesis of *SMARCC1*-variant hydrocephalus, we
7 leveraged the fate patterning of *Xenopus*, in which embryos at the two-cell stage can be
8 selectively injected with MO on one side of the organism and then compared with the opposite
9 side injected with nonsense MO as an isogenic control (see Methods, Fig. 2h). PCNA
10 immunostaining (a marker of cellular proliferation) at stage 46 showed *Smarcc1* variants have
11 significantly fewer PCNA⁺ periventricular cells on the MO-injected side compared to the control
12 side (Fig. 3i-3l). This was particularly evident in the midbrain and tectum, structures situated
13 dorsal and ventral to the aqueduct, respectively. The length of the tectum in *Smarcc1* depleted
14 tissue was markedly reduced and its angulation with the anterior portion of the midbrain was
15 altered, indicating significant dysmorphology or atresia. Forebrain thickness was also
16 significantly reduced on the MO-injected versus the control side (Fig. 3m). These data are
17 consistent with cortical and midbrain dysgenesis secondary to the impaired proliferation of
18 *SMARCC1*-variant NPCs.

19
20 To gain insight into the molecular impact of *SMARCC1* variants in humans, we performed bulk
21 RNA-seq analysis on human frontal and motor-sensory cortex tissue from severely
22 hydrocephalic proband CHYD364-1 (p.Gln575*), who unfortunately underwent fetal demise at
23 PCW 20 (Fig. 4a). We compared these results to a spatial and developmental time-matched
24 RNA-seq control dataset from the BrainSpan database.^{53,82} Analysis of differentially expressed
25 genes (DEGs) identified several genes with significantly higher or lower expression compared to
26 control samples (Fig. 4b, 4c). Gene Ontology (GO) analysis of significantly down-regulated
27 DEGs showed enrichment in multiple terms related to structural neurodevelopment, including
28 ‘nervous system development,’ ‘neurogenesis,’ and ‘regulation of cell development,’ whereas
29 significantly up-regulated DEGs were enriched for terms related to neural transport and signaling
30 (Fig. 4d).

1 Among the most significant DEGs were *NEUROD2* and *MAB21L2*, transcription factors with
2 human orthologues in *Xenopus* which have been shown in both mice and *Xenopus* to play critical
3 roles in brain morphogenesis via NPC regulation⁸³⁻⁸⁶ (Supplementary Fig. 5). Examination of the
4 expression profiles of *NEUROD2* and *MAB21L2* in human prenatal single-cell RNA-sequencing
5 (scRNA-seq) datasets revealed highly enriched expression in intermediate progenitor cells
6 (IPC1), the same cell type with robust *SMARCC1* expression during early brain development
7 (Supplementary Fig. 6). Whole-mount *in situ* hybridization showed MO-mediated *Smarcc1*
8 depletion in the two-cell model (see above) caused a significant reduction of *Neurod2* and
9 *Mab21l2*, on the MO-injected versus control side (Fig. 4e-4g). These results suggest *SMARCC1*
10 variants in CH may cause cortical and midbrain dysgenesis by altering the expression of key
11 transcription factors, including *Neurod2* and *Mab21l2*, that are involved in the regulation of the
12 growth and proliferation of NPCs.

13
14 Given the limitations of studying the brain transcriptome in the very rare scenario of a single
15 human fetus with *SMARCC1* mutation above, we studied a single-cell RNA sequenced (scRNA-
16 seq) atlas of 71,985 individual cells from the brains of age-matched wild-type and *Smarcb1*-
17 mutant mice⁸⁷. The non-truncating variant in *Smarcb1*, encoding a core subunit of the SWI/SNF
18 complex that interacts with *Smarcc1* (Fig. 5a), leads to an elongated *Smarcb1* protein product
19 that causes severe CH with high penetrance during fetal development.

20
21 Consistent with our findings from the patient above, in this model we found *Smarcc1* expression
22 was highly enriched in NPCs in both *Smarcb1*-mutant and wild-type mice. Interestingly,
23 *Smarcc1* had significantly higher expression in NPCs of *Smarcb1*-mutant mice ($p=1.99 \times 10^{-135}$)
24 compared to NPCs in their wild-type counterparts of the same age ($p=3.16 \times 10^{-67}$, Fig. 5b-c).
25 Analysis of DEGs identified genes with significantly higher or lower expression in *Smarcb1*-
26 mutant mice compared to WT; among the highest of these *Neurod2*, as in the human patient (Fig.
27 5d). GO analysis of significantly down-regulated DEGs showed enrichment in multiple terms
28 related to structural neurodevelopment as in the human patient, including ‘brain development’ (p
29 adj. = 3.70×10^{-5}) and ‘axon guidance’ (p adj.= 8.49×10^{-4}) whereas significantly up-regulated
30 DEGs were enriched for terms related to neural precursor replication and differentiation

1 including ‘regulation of stem cell proliferation’ (p adj. = 1.83×10^{-4}) and ‘positive regulation of
2 cellular differentiation’ (p adj. = 1.67×10^{-7}) (Fig. e-f). Together, these findings suggest *Smarcc1*
3 and its interacting SWI/SNF complex components are key regulators of the NPC transcriptome
4 during fetal brain development, and mutational disruption of this pathway in NPCs results in
5 impaired neurogenesis and the development of aqueductal stenosis and cerebral
6 ventriculomegaly and other structural brain defects.

7 **Discussion**

8 Our data provide evidence that DNVs variants in *SMARCC1* cause a novel human syndrome
9 characterized by cerebral ventriculomegaly and aqueductal stenosis, DD, and other associated
10 structural brain and cardiac defects. We propose the name “SMARCC1-associated
11 Developmental Dysgenesis Syndrome (SaDDS)” to describe this novel BAFopathy. These
12 results highlight the importance of SMARCC1 and the BAF chromatin remodeling complex in
13 human brain morphogenesis and provide further support for a “neural stem cell” paradigm of
14 human CH.^{34,35,88,89} These data also demonstrate the power of trio-based WES for identifying
15 pathogenic variants in sporadic structural brain disorders, and suggest WES may be a useful
16 prognostic adjunct when evaluating the surgical candidacy of CH patients.

17
18 The variant spectrum of *SMARCC1* involving its BAF complex-interacting SWIRM, Chromo,
19 and Myb-DNA-binding domains suggests that these variants lead to functional impairment of the
20 BAF complex.^{32,33,66} Indeed, neurodevelopmental disorders (NDDs) with overlapping clinical
21 phenotypes are associated with pathogenic variants in other subunits of the BAF chromatin
22 remodeling complex. Thus, the *SMARCC1*-associated condition presented here partially overlaps
23 with BAFopathies such as CSS and Nicolaides-Baraitser-like syndrome, characterized by ID/DD
24 and neurobehavioral abnormalities. In support of this, several individuals with deleterious
25 *SMARCC1* variants have been reported in other cohorts ascertained on the basis of congenital
26 anomalies, including neural tube defects⁷⁰, autism⁷², or congenital heart disease (CHD)⁷³, and
27 others^{68,69,71} (Supplementary Table 3). However, a defining phenotype of patients with
28 *SMARCC1* variation appears to be cerebral ventriculomegaly associated with aqueductal stenosis
29 that often requires neurosurgical intervention. This phenotype is likely overrepresented in our

1 patients, insofar as recruitment for our cohort was based on the presence of cerebral
2 ventriculomegaly, including those treated with neurosurgery. Nonetheless, other SWI/SNF
3 complex members including *SMARCB1*⁹⁰ and *ARID1A*⁹¹ have been implicated in cerebral
4 ventriculomegaly, and knockout mouse models of *Smarcb1* and *Smarca4*, encoding binding
5 partners of Smarcc1, also exhibit CH^{87,92}, similar to the new *Smarcc1* mutant frogs reported here.
6 These findings support the pathogenicity of the reported *SMARCC1* variants in the pathogenesis
7 of cerebral ventriculomegaly. These findings are in line with the known phenotypic
8 heterogeneity and incomplete penetrance of other BAFopathy genes.^{22,67,68,93} As more patients
9 are collected the full phenotypic spectrum of the human SMARCC1 syndrome will be clarified
10 and genotype-phenotype correlations may arise.

11
12 Our results suggest incomplete penetrance and variable expressivity for some *SMARCC1*
13 variants, a phenomenon well-recognized for other CH and ASD risk genes^{32,94}, as well as for
14 other BAF complex genes.^{22,95-97} Mechanistic drivers of incomplete penetrance and variable
15 expressivity in this specific context remain unclear but may include common genetic or
16 environmental modifiers such as inflammatory or oxidative triggers,^{98,99} as well as stochastic
17 components resulting in mosaicism.¹⁰⁰ As the paralogous *SMARCC1* and *SMARCC2* gene
18 products form hetero- or homodimers¹⁵ and share functional scaffolding properties,²⁸
19 upregulation of *SMARCC2* or other BAF members could compensate for the loss of *SMARCC1*,
20 possibly leading to less severe phenotypes. As different *SMARCC1* isoforms are expressed in
21 different tissues and at different developmental stages^{24,32,82}, both the spatio-temporal profile and
22 isoform of the protein containing the variant could affect the phenotype. Further, the wide
23 phenotypic variety and lack of clear genotype-phenotype correlation characterizing conditions
24 associated with BAF-complex variants suggest possible gene dosage-dependent mechanisms
25 affecting variants of the ATP-dependent chromatin remodeling machinery.¹⁷

26
27 The well-orchestrated spatiotemporal regulation of BAF complex subunit assembly and activity
28 is essential for the development and function of the central nervous system.^{26,101,102} BAF
29 complexes specific to NPCs control cell proliferation, differentiation, and survival through the
30 epigenetic regulation of gene expression that is essential for telencephalon development.^{24,27} We

1 showed *SMARCC1* is highly expressed in fetal human NPCs, and our analysis of a human
2 *SMARCC1*-mutant hydrocephalic fetus suggest *SMARCC1* variants dysregulate the expression
3 of genes critical for neurogenesis, including transcription factors *NEUROD2* and *MAB21L2*.
4 Similar results were derived from our analysis of the scRNAseq atlas of *Smarcb1*-mutant
5 hydrocephalic fetal brains. Interestingly, *Smarcc1* expression was significantly increased in
6 *Smarcb1*-mutant NPCs, perhaps compensating for the depletion of *Smarcb1*. Together, these data
7 suggest *SMARCC1* variants, possibly by altering the epigenetic regulation of gene expression,
8 impair NPC growth and proliferation. Resultant attenuation of neurogenesis and gliogenesis
9 could then lead to non-obstructive (“*ex vacuo*”) ventriculomegaly from a thinned cortical mantle,
10 as has been shown with other CH-associated gene variants,⁸⁸ and obstructive hydrocephalus
11 secondary to midbrain dysgenesis and aqueductal stenosis. The latter is consistent with the fact
12 that normal cerebral aqueduct development requires the precise regulation of the proliferation
13 and differentiation of NPCs and the development of their associated fiber tracts in the
14 mesencephalon following the prenatal closure of the neural tube.¹⁰³⁻¹⁰⁶ Notably, the BAF
15 complex also modulates the expression of cardiac progenitor cells and regulates cardiac
16 remodeling during development and repair.^{11-13,107} Inactivation of the complex has been
17 implicated in cardiac hypertrophy, shortened or incomplete separation of outflow tracts, and
18 persistent truncus arteriosus in rodents.^{11,108} In particular, a p.Lys615Ile frameshift variant in
19 *SMARCC1* has been associated with hypoplastic right or left heart syndrome in humans.⁷³ Recent
20 studies indicate that CHD patients exhibit increased prevalence of neurodevelopmental
21 disabilities, and CHD patients with neurodevelopmental outcomes have a higher burden of
22 damaging DNVs, particularly in genes important to both heart and brain development.¹⁰⁹

23

24 Multiple “impaired brain plumbing” mechanisms have been proposed to account for
25 hydrocephalus, including increased CSF secretion, decreased intraventricular CSF transit from
26 cilia dysfunction, and decreased CSF reabsorption associated with elevated venous pressure,
27 arachnoid granulation immaturity, and lymphatic dysplasia.¹¹⁰ However, accumulating genetic
28 data^{32,94,111,112} suggest that impaired neurogenesis rather than overactive CSF accumulation may
29 underlie some forms of CH. Our findings with *SMARCC1* support such a “neural stem cell”
30 paradigm of disease.^{32,94,111} In the case of patients with variants in *TRIM71* (another CH-
31 associated gene), impaired post-transcriptional silencing of RNA targets leads to decreased NPC

1 proliferation at even earlier time points, resulting in severe cortical hypoplasia and secondary
2 ventriculomegaly.¹¹¹ The opposite phenotype of NPC hyperproliferation due to *PTEN* variant
3 and constitutive activation of the PI3K pathway may also occur.¹¹³

4
5 The diversity of genetic etiologies and underlying biochemical pathways in CH supports the
6 implementation of routine clinical WES for newly diagnosed patients. Current recommendations
7 for workup of fetal and neonatal ventriculomegaly include rapid commercial microarray testing
8 for known chromosomal and copy-number abnormalities.¹¹⁴ However, this strategy does not
9 address CH cases explained by recently detected variants in many new CH genes^{32,33,88}.
10 Application of routine WES or whole genome sequencing could improve the management of
11 children with CH by aiding prognostication and treatment stratification (including when or when
12 not to operate); increasing vigilance for medical screening of variant-associated conditions (such
13 as cancer surveillance for CH patients with variants in *PIK3CA* or *PTEN*); and providing
14 recurrence rates to increase reproductive confidence.

15
16 Our study is limited by the fact our cohort was ascertained on the basis of congenital cerebral
17 ventriculomegaly, including treated hydrocephalus, given previous work in much smaller cohorts
18 suggested a role for *SMARCC1* in these conditions.^{32,33} Continued identification of variant
19 patients will expand our knowledge of the *SMARCC1* phenotypic spectrum, including those
20 patients without ventriculomegaly. Additional patients may also permit genotype-phenotype
21 correlations. In addition, brain tissue for bulk RNA-seq was available from only one human
22 subject, since access to *SMARCC1*-mutated fetal brain is such an exceedingly rare event. Using
23 scRNA-seq on multiple human subjects and inclusion of biological replicates would be a goal of
24 future investigations. Another limitation is the embryonic lethality phenotype of *Smarcc1*
25 knockout mice,^{29,30} which necessitated our use of the non-mammalian *Xenopus* model for disease
26 modeling and mechanistic study.

27
28 These findings have clinical implications. These data suggest that detection of a *de novo*
29 *SMARCC1* variant should trigger a brain MRI in that patient (if not already done) as well as a

1 referral to a clinical geneticist for a systematic phenotypic assessment. However, the risk for
2 future pregnancies for that proband is uncertain given the poorly understood incomplete
3 penetrance and variable expressivity of *SMARCC1* variants. In affected probands found to have a
4 transmitted *SMARCC1* variant from an apparently unaffected carrier parent, a screening brain
5 MRI and a heart ultrasound for the carrier parent and genetic testing for other children, with
6 screening imaging reserved for variant-positive children, could be entertained. Thus, variants in
7 *SMARCC1* should be evaluated on a case-by-case basis for potential monogenic CH
8 pathogenicity, considering individual variant characteristics, patient alignment to the described
9 phenotypic spectrum, and family history of disease. We further encourage the use of and, where
10 applicable, the contribution of data to publicly available resources such as ClinVar, GnomAD,
11 and dbGaP for the evaluation of *SMARCC1* variant pathogenicity at the individual patient level.

12
13 In conclusion, our data suggest pathogenic DNVs in *SMARCC1* variants cause a novel human
14 BAFopathy characterized by DD, cerebral ventriculomegaly, and a variety of structural brain or
15 cardiac defects. These data underscore the importance of *SMARCC1* and the BAF chromatin
16 remodeling complex for human brain morphogenesis and support a neural stem cell paradigm of
17 human CH pathogenesis. These results highlight the power of trio-based WES for identifying
18 risk genes for congenital structural brain disorders and suggest WES may be a valuable adjunct
19 in the management of patients with CH.

21 **Data availability**

22 The data that support the findings of this study will be made available upon reasonable request
23 from kahle.kristopher@mgh.harvard.edu

25 **Acknowledgements**

26 We are grateful to the patients and families who participated in this research.

27

1 **Funding**

2 This work was supported by the Yale-NIH Center for Mendelian Genomics (grant
3 5U54HG006504) and the University of Washington Center for Mendelian Genomics (grants
4 UW-CMG, UM1HG006493, U24HG008956), National Institutes of Health (grants R01
5 NS111029-01A1, R01 NS109358, R01 NS127879-01, R01HL109942, R21 NS116484-02, and
6 K12 228168) (K.K., E.D, S.C.J); the Rudi Schulte Research Institute (K.K.), the National Heart,
7 Lung, and Blood Institute (R00HL143036-02) (S.C.J), the Hydrocephalus Association Innovator
8 Award (E.D., K.K., S.C.J.), the Clinical & Translational Research Funding Program Award
9 (CTSA1405; (S.C.J.), the Children's Discovery Institute Faculty Scholar Award (CDI-FR-2021-
10 926) (S.C.J), and the Eunice Kennedy Shriver National Institute of Child Health and Human
11 Development of the National Institutes of Health (R01HD104938-01A1) (A.M.D).

12

13 **Competing interests**

14 S. McGee and P. Kruszka are employees of GeneDx. All other co-authors have no conflicts of
15 interest to disclose.

16

17 **Supplementary material**

18 Supplementary material will be made available at *Brain* online.

19

20 **References**

- 21 1. Masliah-Planchon J, Bieche I, Guinebretiere JM, Bourdeaut F, Delattre O. SWI/SNF
22 chromatin remodeling and human malignancies. *Annu Rev Pathol.* 2015;10:145-171.
- 23 2. Clapier CR, Cairns BR. The biology of chromatin remodeling complexes. *Annu Rev*
24 *Biochem.* 2009;78:273-304.

- 1 3. Clapier CR, Iwasa J, Cairns BR, Peterson CL. Mechanisms of action and regulation of
2 ATP-dependent chromatin-remodelling complexes. *Nat Rev Mol Cell Biol.*
3 2017;18(7):407-422.
- 4 4. Wang W, Xue Y, Zhou S, Kuo A, Cairns BR, Crabtree GR. Diversity and specialization
5 of mammalian SWI/SNF complexes. *Genes Dev.* 1996;10(17):2117-2130.
- 6 5. Alfert A, Moreno N, Kerl K. The BAF complex in development and disease. *Epigenetics*
7 *Chromatin.* 2019;12(1):19.
- 8 6. Kadoch C, Hargreaves DC, Hodges C, et al. Proteomic and bioinformatic analysis of
9 mammalian SWI/SNF complexes identifies extensive roles in human malignancy. *Nat*
10 *Genet.* 2013;45(6):592-601.
- 11 7. Zhao K, Wang W, Rando OJ, et al. Rapid and phosphoinositol-dependent binding of the
12 SWI/SNF-like BAF complex to chromatin after T lymphocyte receptor signaling. *Cell.*
13 1998;95(5):625-636.
- 14 8. Yan L, Xie S, Du Y, Qian C. Structural Insights into BAF47 and BAF155 Complex
15 Formation. *J Mol Biol.* 2017;429(11):1650-1660.
- 16 9. Yao B, Christian KM, He C, Jin P, Ming GL, Song H. Epigenetic mechanisms in
17 neurogenesis. *Nat Rev Neurosci.* 2016;17(9):537-549.
- 18 10. Yan Z, Wang Z, Sharova L, et al. BAF250B-associated SWI/SNF chromatin-remodeling
19 complex is required to maintain undifferentiated mouse embryonic stem cells. *Stem Cells.*
20 2008;26(5):1155-1165.
- 21 11. Bevilacqua A, Willis MS, Bultman SJ. SWI/SNF chromatin-remodeling complexes in
22 cardiovascular development and disease. *Cardiovasc Pathol.* 2014;23(2):85-91.
- 23 12. Lei I, Liu L, Sham MH, Wang Z. SWI/SNF in cardiac progenitor cell differentiation. *J*
24 *Cell Biochem.* 2013;114(11):2437-2445.
- 25 13. Vieira JM, Howard S, Villa Del Campo C, et al. BRG1-SWI/SNF-dependent regulation
26 of the Wt1 transcriptional landscape mediates epicardial activity during heart
27 development and disease. *Nat Commun.* 2017;8:16034.

- 1 14. Ho L, Jothi R, Ronan JL, Cui K, Zhao K, Crabtree GR. An embryonic stem cell
2 chromatin remodeling complex, esBAF, is an essential component of the core
3 pluripotency transcriptional network. *Proc Natl Acad Sci U S A*. 2009;106(13):5187-
4 5191.
- 5 15. Machol K, Rousseau J, Ehresmann S, et al. Expanding the Spectrum of BAF-Related
6 Disorders: De Novo Variants in SMARCC2 Cause a Syndrome with Intellectual
7 Disability and Developmental Delay. *Am J Hum Genet*. 2019;104(1):164-178.
- 8 16. Hoyer J, Ekici AB, Ende S, et al. Haploinsufficiency of ARID1B, a member of the
9 SWI/SNF-a chromatin-remodeling complex, is a frequent cause of intellectual disability.
10 *Am J Hum Genet*. 2012;90(3):565-572.
- 11 17. Bogershausen N, Wollnik B. Mutational Landscapes and Phenotypic Spectrum of
12 SWI/SNF-Related Intellectual Disability Disorders. *Front Mol Neurosci*. 2018;11:252.
- 13 18. Santen GW, Aten E, Sun Y, et al. Mutations in SWI/SNF chromatin remodeling complex
14 gene ARID1B cause Coffin-Siris syndrome. *Nat Genet*. 2012;44(4):379-380.
- 15 19. Wieczorek D, Bögershausen N, Beleggia F, et al. A comprehensive molecular study on
16 Coffin-Siris and Nicolaides-Baraitser syndromes identifies a broad molecular and clinical
17 spectrum converging on altered chromatin remodeling. *Hum Mol Genet*.
18 2013;22(25):5121-5135.
- 19 20. Sousa SB, Abdul-Rahman OA, Bottani A, et al. Nicolaides-Baraitser syndrome:
20 Delineation of the phenotype. *Am J Med Genet A*. 2009;149a(8):1628-1640.
- 21 21. Mari F, Marozza A, Mencarelli MA, et al. Coffin-Siris and Nicolaides-Baraitser
22 syndromes are a common well recognizable cause of intellectual disability. *Brain Dev*.
23 2015;37(5):527-536.
- 24 22. Van Houdt JK, Nowakowska BA, Sousa SB, et al. Heterozygous missense mutations in
25 SMARCA2 cause Nicolaides-Baraitser syndrome. *Nat Genet*. 2012;44(4):445-449, s441.
- 26 23. DelBove J, Rosson G, Strobeck M, et al. Identification of a core member of the SWI/SNF
27 complex, BAF155/SMARCC1, as a human tumor suppressor gene. *Epigenetics*.
28 2011;6(12):1444-1453.

- 1 24. Nowakowski TJ, Bhaduri A, Pollen AA, et al. Spatiotemporal gene expression
2 trajectories reveal developmental hierarchies of the human cortex. *Science*.
3 2017;358(6368):1318-1323.
- 4 25. Nguyen H, Sokpor G, Pham L, et al. Epigenetic regulation by BAF (mSWI/SNF)
5 chromatin remodeling complexes is indispensable for embryonic development. *Cell*
6 *Cycle*. 2016;15(10):1317-1324.
- 7 26. Sokpor G, Xie Y, Rosenbusch J, Tuoc T. Chromatin Remodeling BAF (SWI/SNF)
8 Complexes in Neural Development and Disorders. *Front Mol Neurosci*. 2017;10:243.
- 9 27. Narayanan R, Pham L, Kerimoglu C, et al. Chromatin Remodeling BAF155 Subunit
10 Regulates the Genesis of Basal Progenitors in Developing Cortex. *iScience*. 2018;4:109-
11 126.
- 12 28. Narayanan R, Pirouz M, Kerimoglu C, et al. Loss of BAF (mSWI/SNF) Complexes
13 Causes Global Transcriptional and Chromatin State Changes in Forebrain Development.
14 *Cell Rep*. 2015;13(9):1842-1854.
- 15 29. Harmacek L, Watkins-Chow DE, Chen J, et al. A unique missense allele of BAF155, a
16 core BAF chromatin remodeling complex protein, causes neural tube closure defects in
17 mice. *Dev Neurobiol*. 2014;74(5):483-497.
- 18 30. Panamarova M, Cox A, Wicher KB, et al. The BAF chromatin remodelling complex is an
19 epigenetic regulator of lineage specification in the early mouse embryo. *Development*.
20 2016;143(8):1271-1283.
- 21 31. Kim JK, Huh SO, Choi H, et al. Srg3, a mouse homolog of yeast SWI3, is essential for
22 early embryogenesis and involved in brain development. *Mol Cell Biol*.
23 2001;21(22):7787-7795.
- 24 32. Furey CG, Choi J, Jin SC, et al. De Novo Mutation in Genes Regulating Neural Stem
25 Cell Fate in Human Congenital Hydrocephalus. *Neuron*. 2018;99(2):302-314 e304.
- 26 33. Jin SC, Dong W, Kundishora AJ, et al. Exome sequencing implicates genetic disruption
27 of prenatal neuro-gliogenesis in sporadic congenital hydrocephalus. *Nat Med*.
28 2020;26(11):1754-1765.

- 1 34. Duy PQ, Rakic P, Alper SL, et al. Brain ventricles as windows into brain development
2 and disease. *Neuron*. 2022;110(1):12-15.
- 3 35. Rodríguez EM, Guerra MM. Neural Stem Cells and Fetal-Onset Hydrocephalus. *Pediatr*
4 *Neurosurg*. 2017;52(6):446-461.
- 5 36. Rodríguez EM, Guerra MM, Vío K, et al. A cell junction pathology of neural stem cells
6 leads to abnormal neurogenesis and hydrocephalus. *Biol Res*. 2012;45(3):231-242.
- 7 37. Krumm N, Turner TN, Baker C, et al. Excess of rare, inherited truncating mutations in
8 autism. *Nat Genet*. 2015;47(6):582-588.
- 9 38. Purcell S, Neale B, Todd-Brown K, et al. PLINK: a tool set for whole-genome
10 association and population-based linkage analyses. *Am J Hum Genet*. 2007;81(3):559-
11 575.
- 12 39. Manichaikul A, Mychaleckyj JC, Rich SS, Daly K, Sale M, Chen WM. Robust
13 relationship inference in genome-wide association studies. *Bioinformatics*.
14 2010;26(22):2867-2873.
- 15 40. Stram DO. Software for tag single nucleotide polymorphism selection. *Hum Genomics*.
16 2005;2(2):144-151.
- 17 41. McKenna A, Hanna M, Banks E, et al. The Genome Analysis Toolkit: a MapReduce
18 framework for analyzing next-generation DNA sequencing data. *Genome Res*.
19 2010;20(9):1297-1303.
- 20 42. Van der Auwera GA, Carneiro MO, Hartl C, et al. From FastQ data to high confidence
21 variant calls: the Genome Analysis Toolkit best practices pipeline. *Curr Protoc*
22 *Bioinformatics*. 2013;43(1110):11.10.11-11.10.33.
- 23 43. Wang K, Li M, Hakonarson H. ANNOVAR: functional annotation of genetic variants
24 from high-throughput sequencing data. *Nucleic Acids Res*. 2010;38(16):e164.
- 25 44. Karczewski KJ, Francioli LC, Tiao G, et al. The mutational constraint spectrum
26 quantified from variation in 141,456 humans. *Nature*. 2020;581(7809):434-443.
- 27 45. Wang YC, Wu Y, Choi J, et al. Computational Genomics in the Era of Precision
28 Medicine: Applications to Variant Analysis and Gene Therapy. *J Pers Med*. 2022;12(2).

- 1 46. Dong C, Wei P, Jian X, et al. Comparison and integration of deleteriousness prediction
2 methods for nonsynonymous SNVs in whole exome sequencing studies. *Hum Mol Genet.*
3 2015;24(8):2125-2137.
- 4 47. Wei Q, Zhan X, Zhong X, et al. A Bayesian framework for de novo mutation calling in
5 parents-offspring trios. *Bioinformatics.* 2015;31(9):1375-1381.
- 6 48. Diab NS, King S, Dong W, et al. Analysis workflow to assess de novo genetic variants
7 from human whole-exome sequencing. *STAR Protoc.* 2021;2(1):100383.
- 8 49. Kaplanis J, Samocha KE, Wiel L, et al. Evidence for 28 genetic disorders discovered by
9 combining healthcare and research data. *Nature.* 2020;586(7831):757-762.
- 10 50. Kent WJ, Sugnet CW, Furey TS, et al. The human genome browser at UCSC. *Genome*
11 *Res.* 2002;12(6):996-1006.
- 12 51. Hao Y, Hao S, Andersen-Nissen E, et al. Integrated analysis of multimodal single-cell
13 data. *Cell.* 2021;184(13):3573-3587.e3529.
- 14 52. Miller JA, Ding SL, Sunkin SM, et al. Transcriptional landscape of the prenatal human
15 brain. *Nature.* 2014;508(7495):199-206.
- 16 53. Li M, Santpere G, Imamura Kawasawa Y, et al. Integrative functional genomic analysis
17 of human brain development and neuropsychiatric risks. *Science.* 2018;362(6420).
- 18 54. Ritchie ME, Phipson B, Wu D, et al. limma powers differential expression analyses for
19 RNA-sequencing and microarray studies. *Nucleic Acids Res.* 2015;43(7):e47.
- 20 55. Alexa A, Rahnenführer J, Lengauer T. Improved scoring of functional groups from gene
21 expression data by decorrelating GO graph structure. *Bioinformatics.* 2006;22(13):1600-
22 1607.
- 23 56. Gerhart J KM. Normal Table of *Xenopus Laevis* (Daudin): A Systematical and
24 Chronological Survey of the Development from the Fertilized Egg Till the End of
25 Metamorphosis. In: 1st ed. New York: Garland Science; 2020.
- 26 57. Lane M, Mis EK, Khokha MK. Obtaining *Xenopus tropicalis* Eggs. *Cold Spring Harb*
27 *Protoc.* 2022;2022(4):Pdb.prot106344.

- 1 58. Deniz E, Mis EK, Lane M, Khokha MK. Xenopus Tadpole Craniocardiac Imaging Using
2 Optical Coherence Tomography. *Cold Spring Harb Protoc.*
3 2022;2022(5):Pdb.prot105676.
- 4 59. Deniz E, Mis EK, Lane M, Khokha MK. CRISPR/Cas9 F0 Screening of Congenital
5 Heart Disease Genes in *Xenopus tropicalis*. *Methods Mol Biol.* 2018;1865:163-174.
- 6 60. Bhattacharya D, Marfo CA, Li D, Lane M, Khokha MK. CRISPR/Cas9: An inexpensive,
7 efficient loss of function tool to screen human disease genes in *Xenopus*. *Dev Biol.*
8 2015;408(2):196-204.
- 9 61. Henrique D, Adam J, Myat A, Chitnis A, Lewis J, Ish-Horowicz D. Expression of a Delta
10 homologue in prospective neurons in the chick. *Nature.* 1995;375(6534):787-790.
- 11 62. Cao J, Spielmann M, Qiu X, et al. The single-cell transcriptional landscape of
12 mammalian organogenesis. *Nature.* 2019;566(7745):496-502.
- 13 63. Jin S, Guerrero-Juarez CF, Zhang L, et al. Inference and analysis of cell-cell
14 communication using CellChat. *Nat Commun.* 2021;12(1):1088.
- 15 64. Barish S, Barakat TS, Michel BC, et al. BICRA, a SWI/SNF Complex Member, Is
16 Associated with BAF-Disorder Related Phenotypes in Humans and Model Organisms.
17 *Am J Hum Genet.* 2020;107(6):1096-1112.
- 18 65. Duran D, Zeng X, Jin SC, et al. Mutations in Chromatin Modifier and Ephrin Signaling
19 Genes in Vein of Galen Malformation. *Neuron.* 2019;101(3):429-443 e424.
- 20 66. Da G, Lenkart J, Zhao K, Shiekhattar R, Cairns BR, Marmorstein R. Structure and
21 function of the SWIRM domain, a conserved protein module found in chromatin
22 regulatory complexes. *Proc Natl Acad Sci U S A.* 2006;103(7):2057-2062.
- 23 67. Santen GW, Aten E, Vulto-van Silfhout AT, et al. Coffin-Siris syndrome and the BAF
24 complex: genotype-phenotype study in 63 patients. *Hum Mutat.* 2013;34(11):1519-1528.
- 25 68. Chen CA, Lattier J, Zhu W, et al. Retrospective analysis of a clinical exome sequencing
26 cohort reveals the mutational spectrum and identifies candidate disease-associated loci
27 for BAFopathies. *Genet Med.* 2022;24(2):364-373.

- 1 69. Kosmicki JA, Samocha KE, Howrigan DP, et al. Refining the role of de novo protein-
2 truncating variants in neurodevelopmental disorders by using population reference
3 samples. *Nat Genet.* 2017;49(4):504-510.
- 4 70. Al Mutairi F, Alzahrani F, Ababneh F, Kashgari AA, Alkuraya FS. A mendelian form of
5 neural tube defect caused by a de novo null variant in SMARCC1 in an identical twin.
6 *Ann Neurol.* 2018;83(2):433-436.
- 7 71. Lefebvre M, Bruel AL, Tisserant E, et al. Genotype-first in a cohort of 95 fetuses with
8 multiple congenital abnormalities: when exome sequencing reveals unexpected fetal
9 phenotype-genotype correlations. *J Med Genet.* 2021;58(6):400-413.
- 10 72. Wilfert AB, Turner TN, Murali SC, et al. Recent ultra-rare inherited variants implicate
11 new autism candidate risk genes. *Nat Genet.* 2021;53(8):1125-1134.
- 12 73. Reuter MS, Chaturvedi RR, Liston E, et al. The Cardiac Genome Clinic: implementing
13 genome sequencing in pediatric heart disease. *Genet Med.* 2020;22(6):1015-1024.
- 14 74. Ho L, Ronan JL, Wu J, et al. An embryonic stem cell chromatin remodeling complex,
15 esBAF, is essential for embryonic stem cell self-renewal and pluripotency. *Proc Natl
16 Acad Sci U S A.* 2009;106(13):5181-5186.
- 17 75. Tuoc TC, Boretius S, Sansom SN, et al. Chromatin regulation by BAF170 controls
18 cerebral cortical size and thickness. *Dev Cell.* 2013;25(3):256-269.
- 19 76. Ninkovic J, Steiner-Mezzadri A, Jawerka M, et al. The BAF complex interacts with Pax6
20 in adult neural progenitors to establish a neurogenic cross-regulatory transcriptional
21 network. *Cell Stem Cell.* 2013;13(4):403-418.
- 22 77. Seo S, Richardson GA, Kroll KL. The SWI/SNF chromatin remodeling protein Brg1 is
23 required for vertebrate neurogenesis and mediates transactivation of Ngn and NeuroD.
24 *Development.* 2005;132(1):105-115.
- 25 78. Chandler RL, Magnuson T. The SWI/SNF BAF-A complex is essential for neural crest
26 development. *Dev Biol.* 2016;411(1):15-24.
- 27 79. Encha-Razavi F, Sonigo P. Features of the developing brain. *Childs Nerv Syst.*
28 2003;19(7-8):426-428.

- 1 80. Dur AH, Tang T, Viviano S, et al. In *Xenopus* ependymal cilia drive embryonic CSF
2 circulation and brain development independently of cardiac pulsatile forces. *Fluids*
3 *Barriers CNS*. 2020;17(1):72.
- 4 81. Date P, Ackermann P, Furey C, et al. Visualizing flow in an intact CSF network using
5 optical coherence tomography: implications for human congenital hydrocephalus. *Sci*
6 *Rep*. 2019;9(1):6196.
- 7 82. Kang HJ, Kawasawa YI, Cheng F, et al. Spatio-temporal transcriptome of the human
8 brain. *Nature*. 2011;478(7370):483-489.
- 9 83. Lee JE, Hollenberg SM, Snider L, Turner DL, Lipnick N, Weintraub H. Conversion of
10 *Xenopus* ectoderm into neurons by NeuroD, a basic helix-loop-helix protein. *Science*.
11 1995;268(5212):836-844.
- 12 84. Wullimann MF, Rink E, Vernier P, Schlosser G. Secondary neurogenesis in the brain of
13 the African clawed frog, *Xenopus laevis*, as revealed by PCNA, Delta-1, Neurogenin-
14 related-1, and NeuroD expression. *J Comp Neurol*. 2005;489(3):387-402.
- 15 85. Olson JM, Asakura A, Snider L, et al. NeuroD2 is necessary for development and
16 survival of central nervous system neurons. *Dev Biol*. 2001;234(1):174-187.
- 17 86. Wong RL, Chan KK, Chow KL. Developmental expression of Mab2112 during mouse
18 embryogenesis. *Mech Dev*. 1999;87(1-2):185-188.
- 19 87. Brugmans AK, Walter C, Moreno N, et al. A Carboxy-terminal Smarcb1 Point Mutation
20 Induces Hydrocephalus Formation and Affects AP-1 and Neuronal Signalling Pathways
21 in Mice. *Cell Mol Neurobiol*. 2023.
- 22 88. Duy PQ, Weise SC, Marini C, et al. Impaired neurogenesis alters brain biomechanics in a
23 neuroprogenitor-based genetic subtype of congenital hydrocephalus. *Nat Neurosci*.
24 2022;25(4):458-473.
- 25 89. Duy PQ, Rakic P, Alper SL, et al. A neural stem cell paradigm of pediatric
26 hydrocephalus. *Cereb Cortex*. 2022.

- 1 90. Diets IJ, Prescott T, Champaigne NL, et al. A recurrent de novo missense pathogenic
2 variant in SMARCB1 causes severe intellectual disability and choroid plexus hyperplasia
3 with resultant hydrocephalus. *Genet Med.* 2019;21(3):572-579.
- 4 91. Slavotinek A, Lefebvre M, Brehin AC, et al. Prenatal presentation of multiple anomalies
5 associated with haploinsufficiency for ARID1A. *Eur J Med Genet.* 2022;65(2):104407.
- 6 92. Cao M, Wu JI. Camk2a-Cre-mediated conditional deletion of chromatin remodeler Brg1
7 causes perinatal hydrocephalus. *Neurosci Lett.* 2015;597:71-76.
- 8 93. Rive Le Gouard N, Nicolle R, Lefebvre M, et al. First reports of fetal SMARCC1 related
9 hydrocephalus. *Eur J Med Genet.* 2023;66(8):104797.
- 10 94. Jin SC, Dong W, Kundishora AJ, et al. Exome sequencing implicates genetic disruption
11 of prenatal neuro-gliogenesis in sporadic congenital hydrocephalus. *Nat Med.*
12 2020;26(11):1754-1765.
- 13 95. Santen GW, Aten E, Vulto-van Silfhout AT, et al. Coffin-Siris syndrome and the BAF
14 complex: genotype-phenotype study in 63 patients. *Hum Mutat.* 2013;34(11):1519-1528.
- 15 96. Cappuccio G, Sayou C, Tanno PL, et al. De novo SMARCA2 variants clustered outside
16 the helicase domain cause a new recognizable syndrome with intellectual disability and
17 blepharophimosis distinct from Nicolaides-Baraitser syndrome. *Genet Med.*
18 2020;22(11):1838-1850.
- 19 97. Kaufman L, Ayub M, Vincent JB. The genetic basis of non-syndromic intellectual
20 disability: a review. *J Neurodev Disord.* 2010;2(4):182-209.
- 21 98. Morrison AJ. Chromatin-remodeling links metabolic signaling to gene expression. *Mol*
22 *Metab.* 2020;38:100973.
- 23 99. Kenneth NS, Mudie S, van Uden P, Rocha S. SWI/SNF regulates the cellular response to
24 hypoxia. *J Biol Chem.* 2009;284(7):4123-4131.
- 25 100. D'Gama AM, Walsh CA. Somatic mosaicism and neurodevelopmental disease. *Nat*
26 *Neurosci.* 2018;21(11):1504-1514.
- 27 101. Ronan JL, Wu W, Crabtree GR. From neural development to cognition: unexpected roles
28 for chromatin. *Nat Rev Genet.* 2013;14(5):347-359.

- 1 102. Son EY, Crabtree GR. The role of BAF (mSWI/SNF) complexes in mammalian neural
2 development. *Am J Med Genet C Semin Med Genet.* 2014;166c(3):333-349.
- 3 103. Jellinger G. Anatomopathology of non-tumoral aqueductal stenosis. *J Neurosurg Sci.*
4 1986;30(1-2):1-16.
- 5 104. Takashima S, Fukumizu M. [Pathology of congenital aqueductal stenosis and
6 posthemorrhagic hydrocephalus]. *No To Hattatsu.* 1994;26(3):216-221.
- 7 105. Cinalli G, Spennato P, Nastro A, et al. Hydrocephalus in aqueductal stenosis. *Child's*
8 *Nervous System.* 2011;27(10):1621.
- 9 106. Tully HM, Dobyns WB. Infantile hydrocephalus: a review of epidemiology,
10 classification and causes. *Eur J Med Genet.* 2014;57(8):359-368.
- 11 107. Wiley MM, Muthukumar V, Griffin TM, Griffin CT. SWI/SNF chromatin-remodeling
12 enzymes Brahma-related gene 1 (BRG1) and Brahma (BRM) are dispensable in multiple
13 models of postnatal angiogenesis but are required for vascular integrity in infant mice. *J*
14 *Am Heart Assoc.* 2015;4(4).
- 15 108. Mehrotra A, Joe B, de la Serna IL. SWI/SNF chromatin remodeling enzymes are
16 associated with cardiac hypertrophy in a genetic rat model of hypertension. *J Cell*
17 *Physiol.* 2013;228(12):2337-2342.
- 18 109. Homsy J, Zaidi S, Shen Y, et al. De novo mutations in congenital heart disease with
19 neurodevelopmental and other congenital anomalies. *Science.* 2015;350(6265):1262-
20 1266.
- 21 110. Govaert P, Oostra A, Matthys D, Vanhaesebrouck P, Leroy J. How idiopathic is
22 idiopathic external hydrocephalus? *Dev Med Child Neurol.* 1991;33(3):274-276.
- 23 111. Duy PQ, Weise SC, Marini C, et al. Impaired neurogenesis alters brain biomechanics in a
24 neuroprogenitor-based genetic subtype of congenital hydrocephalus. *Nat Neurosci.*
25 2022;25(4):458-473.
- 26 112. Kundishora AJ, Singh AK, Allington G, et al. Genomics of human congenital
27 hydrocephalus. *Childs Nerv Syst.* 2021;37(11):3325-3340.

- 1 113. DeSpensa T, Jr., Carlson M, Panchagnula S, et al. PTEN mutations in autism spectrum
 2 disorder and congenital hydrocephalus: developmental pleiotropy and therapeutic targets.
 3 *Trends Neurosci.* 2021;44(12):961-976.
- 4 114. Etchegaray A, Juarez-Peñalva S, Petracchi F, Igarzabal L. Prenatal genetic considerations
 5 in congenital ventriculomegaly and hydrocephalus. *Childs Nerv Syst.* 2020;36(8):1645-
 6 1660.

8 **Figure legends**

9 **Figure 1 *SMARCC1* mutations are associated with congenital hydrocephalus (CH) and**
 10 **cause a novel human BAFopathy featuring cerebral ventriculomegaly.** (A) Quantile–
 11 quantile (Q-Q) plot of observed versus expected *P*-values for DNVs in each gene in 2,697 trio
 12 cases. *P*-values were calculated using a one-sided Poisson test (see Methods). For protein-
 13 damaging *de novo SMARCC1* variants (LoF, MetaSVM = D, and/or MPC > 2), $p = 5.83 \times 10^{-9}$.
 14 (B) Schematic diagram showing variant locations in *SMARCC1* protein domains. DNVs are
 15 indicated with red markers, transmitted and unknown inheritance variants^{32,33} are indicated with
 16 gray markers. Asterisk indicates recurrent variant. (C) Brain MRIs of CH patients with
 17 *SMARCC1* variants demonstrate consistent structural abnormalities. Prenatal imaging is shown
 18 for patients 115-1 (contrast MRI), 101-1, and 111-1. Red asterisks denote ventricular catheter of
 19 a ventriculo-peritoneal shunt used to treat obstructive hydrocephalus. (D) p.Asp675Gly was
 20 predicted to be detrimental to *SMARCC1* structure and function by Alpha-Fold biophysical
 21 modelling. Structural protein modeling predicts that p.Asp675Gly alters a conserved residue in
 22 the Myb domain resulting in loss of an ion pair interaction with p.Arg602, with a predicted ΔG
 23 of 0.73 kcal/mol.

24
 25 **Figure 2 *SMARCC1* is expressed in intermediate progenitors of the cortical lamina during**
 26 **human brain development.** (A) Analyzed transcriptomic dataset²⁴ showing MAP clustering of
 27 developmental human brain cells, colored by cell type. Early and late born excitatory neuron
 28 PFC (EN-PFC), early and late born excitatory neuron V1 (EN-V1), CGE/LGE-derived inhibitory
 29 neurons (IN-CTX-CGE), MGE-derived ctx inhibitory neuron (IN-CTX-MGE), striatal neurons

1 (IN-STR), dividing intermediate progenitor cells RG-like (IPC-div), intermediate progenitor
 2 cells EN-like (IPC-nEN), dividing MGE progenitors (MGE-div), MGE progenitors (MGE-IPC),
 3 MGE radial glia (MGE-RG), mural/pericyte (Mural), newborn excitatory neuron - early born
 4 (nEN-early), newborn excitatory neuron - late born (nEN-late), MGE newborn neurons (nIN),
 5 oligodendrocyte progenitor cell (OPC), outer radial glia (oRG), dividing radial glia (RG-div),
 6 earlyvRG (RG-early), truncated Radial Glia (tRG), Unknown (U), Ventricular Radial Glia
 7 (vRG). Expression in neural progenitors is featured in red circles. (A) Analyzed transcriptomic
 8 dataset²⁴ showing enrichment analysis across cell type markers of the developmental human
 9 brain for genes with rare risk variation in autism, developmental disorders, congenital heart
 10 disease, and congenital hydrocephalus compared to BAF Complex Genes. Tiles labeled with
 11 $-\log_{10}(P \text{ value})$ and an asterisk represent significant enrichment at the Bonferroni multiple-
 12 testing cutoff ($\alpha = 0.05/23 = 2.17 \times 10^{-3}$). (C) Temporal gene expression profiles for *SMARCC1*
 13 and other BAF Complex genes between post-conception weeks (PCW) 5-36. (D) Analyzed
 14 transcriptomic dataset²⁴ showing heatmap of gene expression levels for *SMARCC1* and other
 15 BAF complex genes across different developmental timepoints. Vertical axis shows timepoints
 16 in post-conception weeks. (E) Analyzed transcriptomic dataset²⁴ showing heatmap of gene
 17 expression levels for for *SMARCC1* and other BAF complex genes across different brain regions.
 18 V1, primary visual cortex; PFC, prefrontal cortex; MGE, medial ganglionic eminence; LGE,
 19 lateral ganglionic eminence; M1 primary motor cortex. (F) Analyzed transcriptomic dataset²⁴
 20 showing heatmap of gene expression levels for for *SMARCC1* and other BAF complex genes
 21 across cortical lamina, PCW 5-40. CP, cortical plate; GZ, germinal zone; VZ, ventricular zone;
 22 SVZ, subventricular zone.

23

24 **Figure 3 *SMARCC1* mutation causes hydrocephalus by disrupting midbrain architecture in**
 25 ***X. tropicalis*.** (A) Mid-sagittal view of the *Xenopus* ventricular system. Dotted white lines
 26 indicate boundaries between labeled regions: tel, telencephalon; di, diencephalon; mes,
 27 mesencephalon; rhomb, rhombencephalon; L, lateral ventricle; III, third ventricle; M, midbrain
 28 ventricle; IV, fourth ventricle. Representative mid-sagittal views for experimental conditions (G0
 29 variant from morpholino oligo, G0 variant from CRISPR #1, G0 variant from CRISPR #2, and
 30 G1 variant progeny from *Smarcc1* MO animals) are shown with aqueductal occlusion marked by
 31 arrows. (B) Quantification of % aqueductal stenosis in uninjected controls (UIC); Cas9 control,

1 and control MO, as well as in the experimental conditions *Smarcc1* MO, *Smarcc1* CRISPR #1,
2 *Smarcc1* CRISPR #2, and *Smarcc1* G1 variant. Data are shown as mean +/- SEM. Open circles
3 indicate the number of experiments, with animal counts indicated above each column.
4 Significance was calculated by one-way ANOVA; **** indicates $p \leq 0.0001$. (C) Quantification
5 of rescue of aqueductal stenosis phenotype with *Smarcc1* MO + WT mRNA ($p = 0.0024$) with
6 recapitulation of phenotype by pathogenic mRNA from p. Q575* variant ($p = 0.4888$). Data are
7 shown as mean +/- SEM. Open circles indicate number of experiments, with animal counts
8 indicated above each column. Significance was calculated by Mann-Whitney test. (D)
9 Representative *X. tropicalis* cardiac OCT image on ventral-dorsal axis, the ventral three chamber
10 view (VTCV). Labeled structures are myocardium, ventricle, L atrium, AV valve, and cardiac
11 sack. (E) Representative cardiac measurements by OCT shown for UIC and *smarcc1* MO. EDD,
12 end diastolic diameter; ESD, end systolic diameter. (F) Quantification of EDD in UIC, Cas9
13 control, and control MO, as well as experimental conditions *smarcc1* MO, *smarcc1* CRISPR #1,
14 *smarcc1* CRISPR #2. Data are shown as Mean +/- SEM. Significance was calculated by One-
15 way ANOVA using GraphPad Prism where $p \leq 0.0001$ for ****. (G) Quantification of ESD in
16 UIC, Cas9 control, and control MO, as well as experimental conditions *smarcc1* MO, *smarcc1*
17 CRISPR #1, *smarcc1* CRISPR #2. Data are shown as Mean +/- SEM. Significance was
18 calculated by one-way ANOVA using GraphPad Prism where $p \leq 0.0001$ for ****. (H)
19 Schematic of two-cell injection protocol in *X. tropicalis*. (I) Labeled representative fluorescence
20 microscopy of WT stage 46 *X. tropicalis* stained with Hoechst. Olfactory bulb, forebrain,
21 midbrain, optic tectum, and cerebellum are indicated. (J) Representative immunofluorescence
22 images of right side-injected control MO and right side-injected *Smarcc1* MO stage 46 *X.*
23 *tropicalis* for PCNA (red) and merged images (with Hoechst, blue). Scale bar represents 500 um.
24 Schematic and chart for quantification of average PCNA intensity ratio for control and *smarcc1*
25 MO injected on the right side with left side un-injected, $p \leq 0.0001$ with unpaired t-test. Data are
26 shown as mean +/- SEM. (K) Schematic and chart for quantification of optic tectum length ratio
27 for WT control and *Smarcc1* MO injected on the right side with left side un-injected, $p \leq 0.0001$
28 with unpaired t-test. Data are shown as mean +/- SEM. (L) Schematic and chart for
29 quantification of optic tectum angulation ratio for WT control and *Smarcc1* MO injected on the
30 right side with left side un-injected, $p = 0.0008$ with unpaired t-test. Data are shown as mean +/-
31 SEM. (M) Schematic and chart for quantification of telencephalon width ratio for WT control

1 and *Smarcc1* MO injected on the right side with left side un-injected, $p = 0.0019$ with unpaired t-
 2 test. Data are shown as mean \pm SEM.

3
 4 **Figure 4 *SMARCC1* mutation dysregulates transcription factors involved in intermediate**
 5 **progenitor biology in human and *X. tropicalis*.** (A) Prenatal ultrasound imaging for patient
 6 CHYD364-1 demonstrates severe cerebral ventriculomegaly and aqueductal stenosis. (B)
 7 Median fold-change of top 20 differentially-expressed genes. *NEUROD2* and *MAB21L2* are
 8 highlighted. (C) Dot plot showing differentially expressed genes between *SMARCC1* variant and
 9 control CTX samples. Each dot represents a gene. The x and y axes represent average gene
 10 expression in control and variant samples, respectively. Genes with a fold change >5 between
 11 samples are in black; others are in grey. *MAB21L2* and *NEUROD2* are highlighted with text. (D)
 12 GO analysis of CH risk genes, including ranked and selected terms. Significance was calculated
 13 by two-sided Fisher's exact test. Scale bar 500 μ m. (E) Representative photomicrograph of DNA
 14 *in situ* hybridization showing *Smarcc1* expression in WT stage 46 of *X. tropicalis*. The forebrain,
 15 midbrain, and hindbrain are indicated. Scale bar represents 500 μ m. (F) Representative
 16 photomicrographs of DNA *in situ* hybridization showing *Neurod2* expression in stage 46 *X.*
 17 *tropicalis*, control and *Smarcc1* MO-injected on the right side, with left side un-injected.
 18 Quantification of forebrain expression area is shown, $p \leq 0.0001$ with unpaired t-test. Data are
 19 shown as means \pm SEM. Scale bar represents 500 μ m. (G) Representative photomicrographs of
 20 DNA *in situ* hybridization showing *Mab21l2* expression and quantification as in F. Scale bar
 21 represents 500 μ m.

22
 23 **Figure 5 Altered *Smarcc1* expression in NPCs and disrupted neurogenesis in *Smarcb1*-**
 24 **mutant hydrocephalic mice.** (A) Schematic of the human SWI/SNF complex, highlighting
 25 SMARCC1 and SMARCB1, core subunits of the complex. (B) Differential expression of
 26 *Smarcc1* and *Smarcb1* by cell type in *Smarcb1*-mutant mice. Significant values are labeled
 27 numerically. (C) Representation of positively and negatively differentially-expressed genes
 28 (DEGs) by log(fold-change) in hydrocephalic *Smarcb1*-mutant mice relative to wild-type.
 29 *Neurod2* is highlighted. (D) *Smarcb1*-mutant positively and negatively DEGs GO biological
 30 processes. Vertical green line indicates statistical significance corrected by the Benjamini-

1 Hochberg method. (E) *Smardcb1*-mutant neuroprogenitor cell-type marker GO biological
 2 processes and molecular functions. Vertical green line indicates statistical significance corrected
 3 by the Benjamini-Hochberg method.
 4

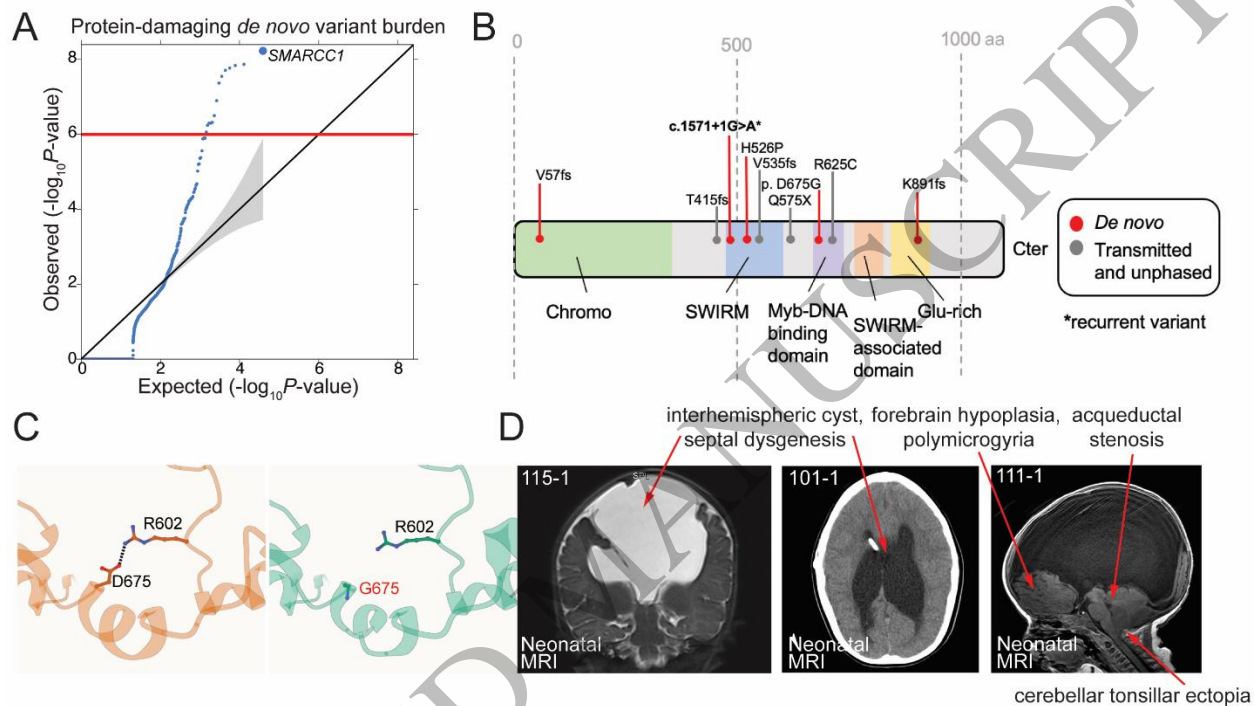


Figure 1
 216x132 mm (x DPI)

5
 6
 7
 8

ACCEPTED

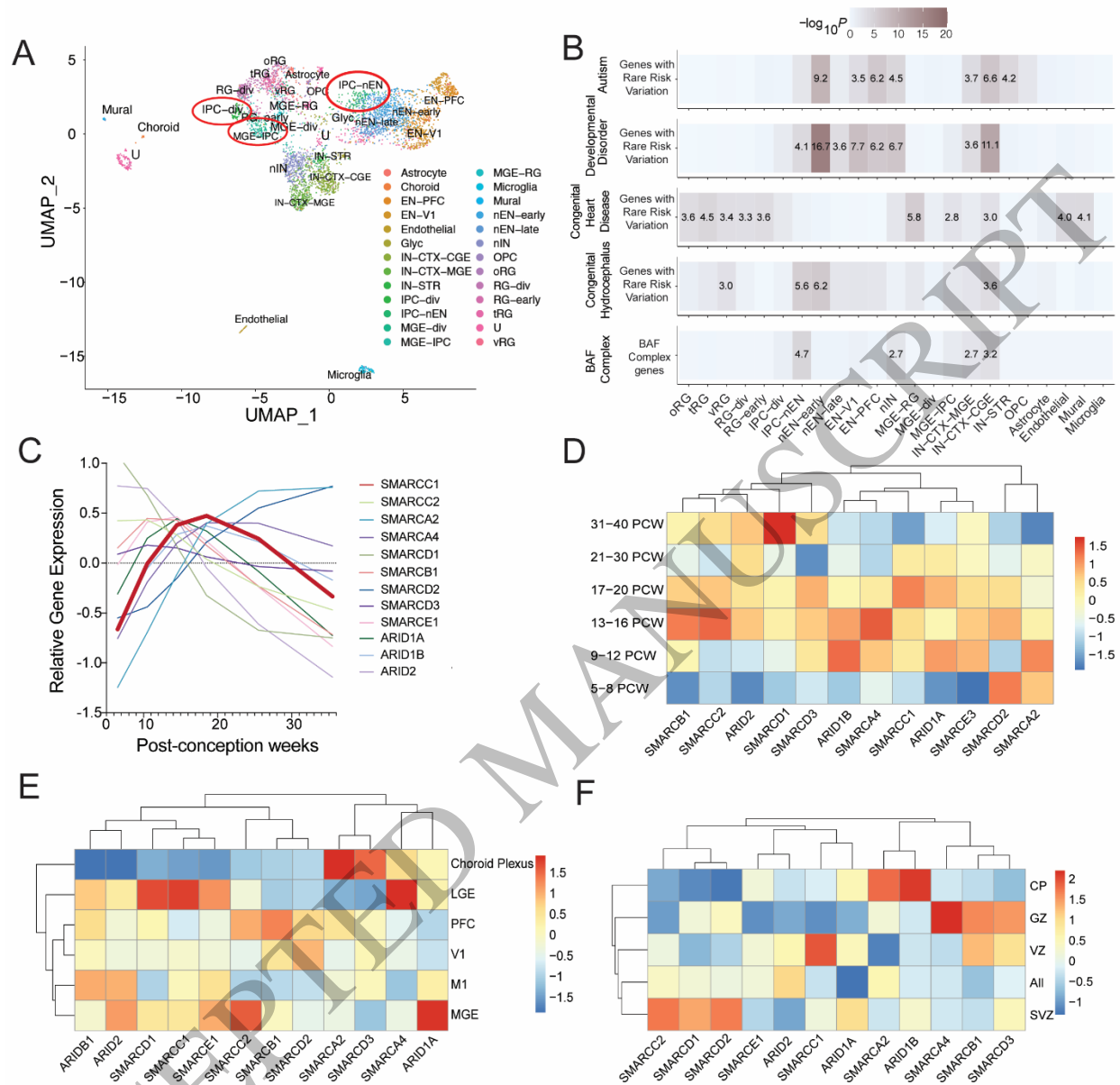


Figure 2
216x213 mm (x DPI)

1
2
3
4

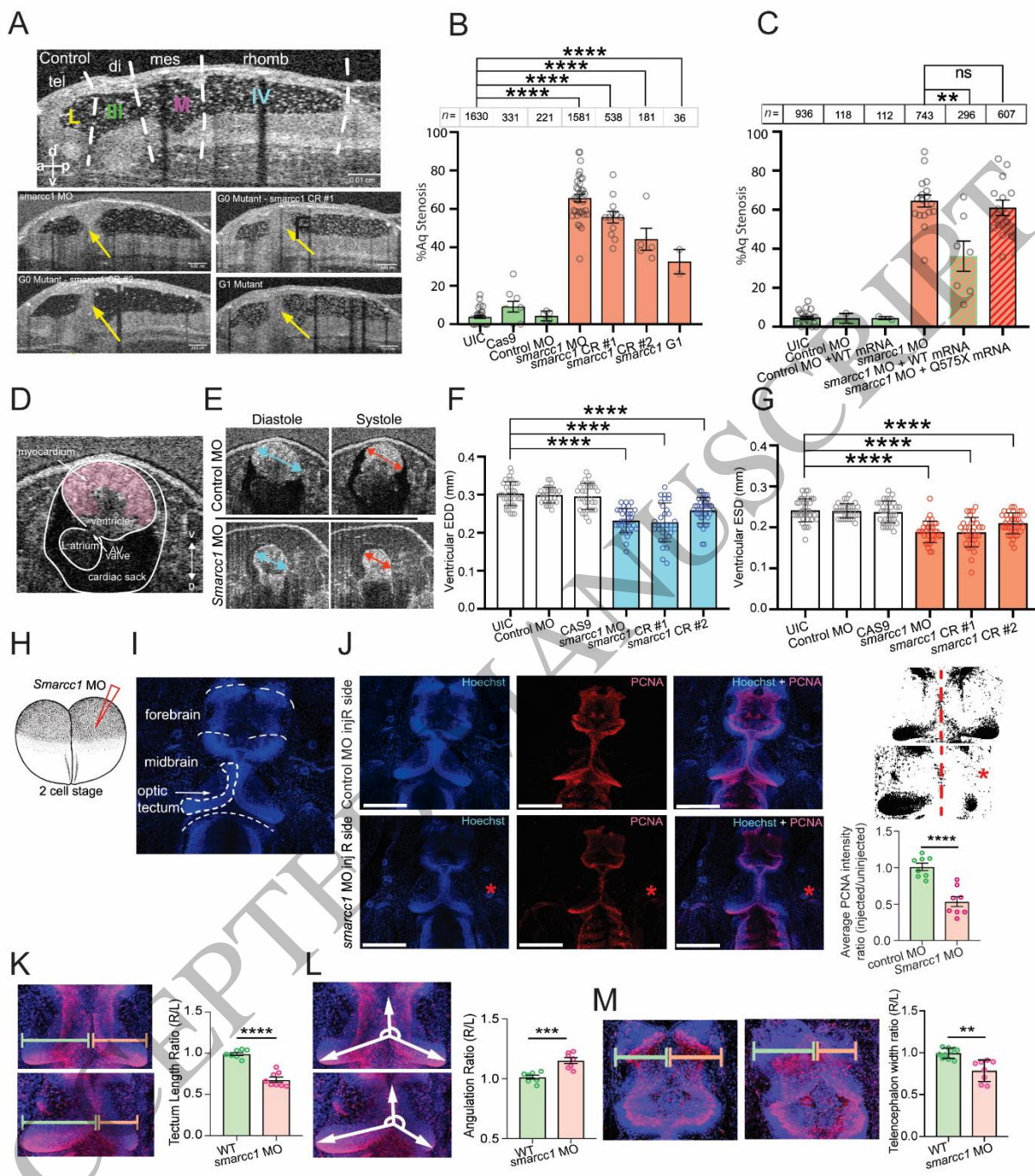


Figure 3
216x238 mm (x DPI)

1
2
3
4

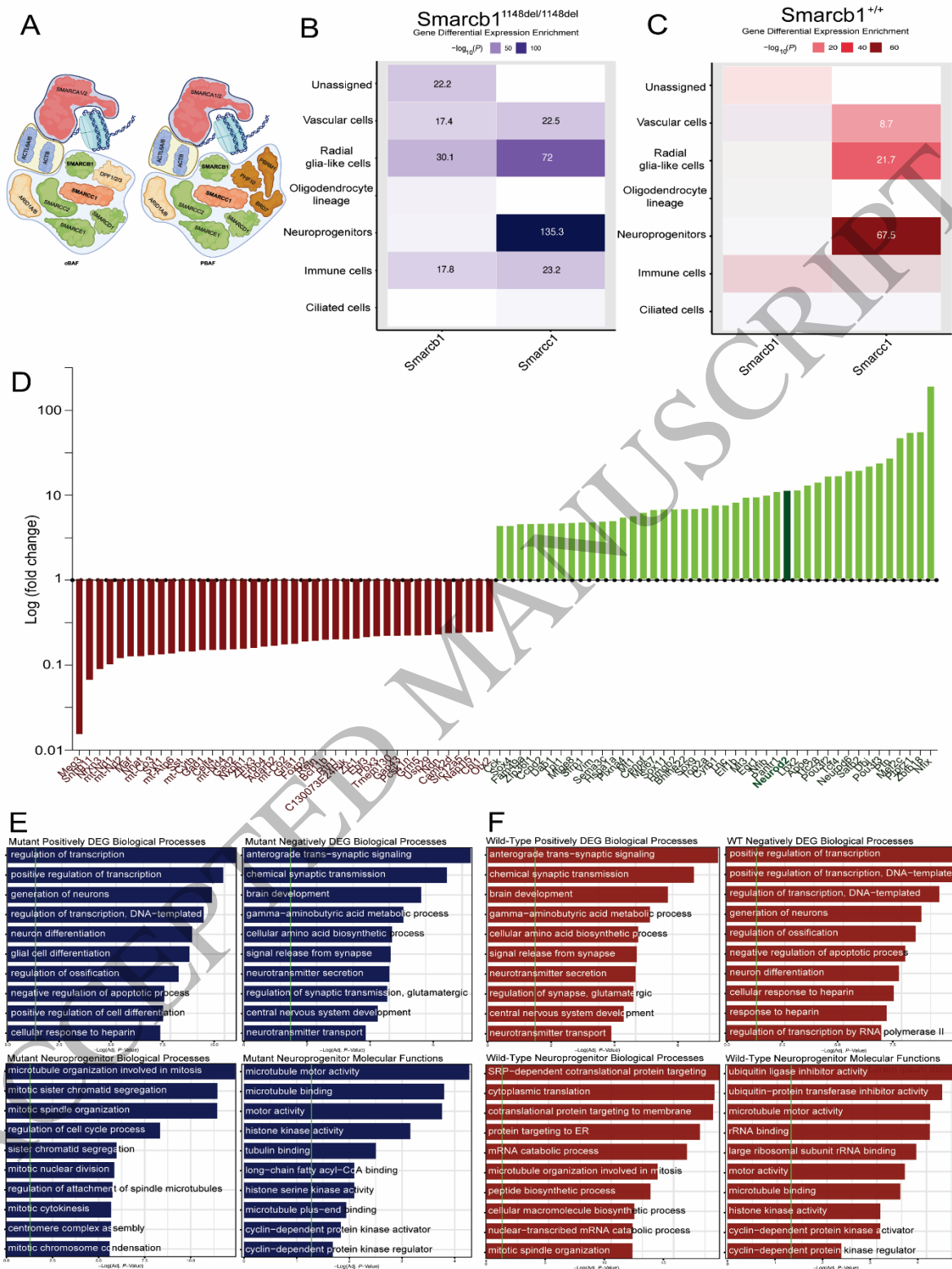


Figure 5
234x338 mm (x DPI)

1
2
3
4

DX3- 1 ^b	<i>novo</i>		Alafs ^c 97)										
Total				(9/10)	(9/10)	(9/10)	(5/10)	(5/10)	(2/10)	(9/10)	(4/10)	(7/10)	(3/10)

- 1 Each plus symbol is equivalent to one instance of the phenotype.
- 2 ^aProbands harboring variants that have been previously reported ^{32,33}
- 3 ^bPhenotypic data for these probands was obtained in aggregate

ACCEPTED MANUSCRIPT